Contrib Mineral Petrol (2011) 162:889–907
DOI 10.1007/s00410-011-0630-7

ORIGINAL PAPER

Metasomatized lithospheric mantle beneath Turkana depression in southern Ethiopia (the East Africa Rift): geochemical and Sr–Nd–Pb isotopic characteristics

Daniel Meshesha · Ryuichi Shinjo · Risa Matsumura · Takele Chekol

Received: 19 November 2010 / Accepted: 21 March 2011 / Published online: 1 April 2011

Abstract Mantle xenoliths entrained in Quaternary alkaline basalts from the Turkana Depression in southern Ethiopia (the East Africa Rift) were studied for their geochemical and Sr–Nd–Pb isotopic compositions to constrain the evolution of the lithosphere. The investigated mantle xenoliths are spinel lherzolites in composition with a protogranular texture. They can be classified into two types: anhydrous and hydrous spinel lherzolites; the latter group characterized by the occurrences of pargasite and phlogopite. The compositions of whole-rock basaltic component (CaO = 3.8–5.6 wt%, Al_2O_3 = 2.5–4.1 wt%, and MgO = 34.7–38.1 wt%), spinel (Cr# = 0.062–0.117, Al_2O_3 = 59.0–64.4 wt%) and clinopyroxene (Mg# = 88.4–91.7, Al_2O_3 = 5.2–6.7 wt%) indicate that the lherzolites are fertile and have not experienced significant partial melting. Both types are characterized by depleted $^{87}Sr/^{86}Sr$ (0.70180–0.70295) and high $^{143}Nd/^{144}Nd$ (0.51299–0.51348) with wide ranges of $^{206}Pb/^{204}Pb$ (17.86–19.68) isotopic compositions. The variations of geochemical and isotopic compositions can be explained by silicate metasomatism induced by different degree of magma infiltrations from ascending mantle plume. The thermobarometric estimations suggest that the spinel lherzolites were derived from depths of 50–70 km (15.6–22.2 kb) and entrained in the alkaline magma at 847–1,052°C. Most of the spinel lherzolites from this study record an elevated geotherm (60–90 mW/m^2) that is related to the presence of rising mantle plume in an active tectonic setting. Sm–Nd isotopic systematic gives a mean T_{DM} model age of 0.95 Ga, interpreted as the minimum depletion age of the subcontinental lithosphere beneath the region.

Keywords Mantle xenoliths · Spinel lherzolites · Metasomatism · Protogranular · Fertile mantle · East African Rift

Communicated by T. L. Grove.

Electronic supplementary material The online version of this article (doi:10.1007/s00410-011-0630-7) contains supplementary material, which is available to authorized users.

D. Meshesha (✉) · R. Shinjo · R. Matsumura · T. Chekol
Department of Physics and Earth Sciences,
University of the Ryukyus, Senbaru-1, Nishihara,
Okinawa 903-0213, Japan
e-mail: am_daniel2002@yahoo.com

Present Address:
R. Matsumura
Center for Crustal Petrology, Department of Earth Sciences,
Stellenbosch University, Privet Bag X1,
Matieland 7602, South Africa

T. Chekol
Pheasant Memorial Laboratory, Institute for Study of the Earth's Interior, Okayama University at Misasa, Tottori 682-0193, Japan

Introduction

Mantle xenoliths were carried to the earth's surface by the rising magma from their depth of formation and are mostly hosted by alkaline lavas (e.g., Xu et al. 2003; Bjerg et al. 2005; Schilling et al. 2005) and kimberlites (e.g., Franz et al. 1996; Boyd et al. 1997; MacKenzie and Canil 1998; Grégoire et al. 2003, 2005). They have been the focus of many intensive studies, because mantle xenoliths can provide direct evidences for upper mantle compositions to a better understanding of the geodynamic evolution of the lithosphere at the time of their eruption (e.g., Frey and

Prinz 1978; Dawson 1984; Boyd 1989; Arai 1994; Rivalenti et al. 1996; Xu et al. 2003; Niu 2004).

In the East African Rift System (EARS; Fig. 1a), plume-related Cenozoic alkaline basalts are widespread and contain different types of crustal and mantle xenoliths that had been brought to the surface during their ascent (e.g., Roger et al. 1999; Rooney et al. 2005; Kaeser et al. 2006; Teklay et al. 2010). Several localities have been reported in the Ethiopian volcanic province for their mantle xenoliths hosted in alkaline basalts, including the southern Ethiopia (Mega, Morten et al. 1992; Bedini et al. 1997; Bedini and Bodinier 1999; Lorand et al. 2003; Reisberg et al. 2004: Mega-Megado, Conticelli et al. 1999), central Main Ethiopian Rift (Debre Zeyit and Butajira, Rooney et al. 2005), and the northwestern Ethiopia (Injibara-Merāwi, Conticelli et al. 1999; Injibara, Roger et al. 1997, 1999; Ayalew et al. 2003; Ferrando et al. 2008; Frezzotti et al. 2010; Simien shield volcano, Ayalew et al. 2009). Except for those in the Miocene alkaline basalts (Ayalew et al. 2009), most of the mantle xenoliths are hosted in Quaternary alkaline basalts. Previous studies have shown that mantle xenoliths beneath the Ethiopian volcanic province are mostly peridotite in compositions and represent a lithosphere that has experienced different degree of partial melting, recrystallization, and metasomatism. These processes are interpreted as the result of thermo-mechanical erosion of the lithosphere above a mantle plume (e.g., Bedini et al. 1997; Bedini and Bodinier 1999; Lorand et al. 2003; Reisberg et al. 2004) or interaction between the lithosphere and fluid and/or magma released from the deeper mantle plume (Conticelli et al. 1999; Rooney et al. 2005; Shinjo and Matsumura 2006; Ferrando et al. 2008).

In this paper, we report results of petrography and mineral and whole-rock chemistry, of seven fresh spinel lherzolite samples hosted in Quaternary basanite-dominated alkaline lavas (1.9–0.3 Ma, Shinjo et al. 2010) from Mega, Dilo, and Goraye areas (Fig 1b), together with Sr–Nd–Pb isotope compositions of clinopyroxene and amphibole separates. Despite the availability of considerable published minerals and whole-rock chemistry for peridotite xenoliths from the Ethiopian volcanic province, it is noteworthy to mention that Sr–Nd–Pb isotope compositions of peridotite xenoliths from this region have not been published. Our dataset has been used to (1) define the geochemical features of lithospheric mantle beneath the Turkana Depression as recorded by the spinel lherzolites, (2) constrain the dominant processes that responsible for the variability of the spinel lherzolites chemistry, and (3) assess the evolution of the lithosphere within the broad rift zone (plume-lithosphere interaction). Furthermore, integrating with previously published data on peridotite xenoliths, we will discuss the diversity and evolution of the lithosphere beneath EARS.

Geological setting

Plume(s)-related uplift and magmatism in the east Africa have produced the Ethiopian and East African plateaus, which are subsequently bisected by active Main Ethiopian Rift (MER) and Eastern (Kenya or Gregory) Rift, respectively (Fig. 1a). These plateaus, manifestation of asthenospheric upwelling, are separated by 300-km wide "broadly rifted zone" (Davidson and Rex 1980) or Turkana Depression (Fig. 1a). The Turkana Depression is a polyphased rift system related to the reactivation of NW–SE trending Mesozoic Anza Graben by NE–SW trending Cenozoic EARS, and it is mainly characterized by the occurrence of episodic magmatism within the EARS section (e.g., Stewart and Rogers 1996; George and Rogers 2002; Furman et al. 2006a).

Although Turkana Depression lacks topographic manifestation of asthenospheric upwelling, many geophysical studies revealed low-velocity anomalies related to anomalously hot and buoyant mantle upwelling beneath various parts of EARS (e.g., Ebinger et al. 1989; Nyblade et al. 2000; Debayle et al. 2001; Benoit et al. 2006a). The low-velocity anomalies are attributed to one or two mantle plumes (e.g., Ebinger and Sleep 1998; George et al. 1998; Rogers et al. 2000) or broad mantle upwelling (African superplume, Janney et al. 2002; Furman et al. 2004, 2006b) that caused lithospheric thinning beneath EARS. An investigation of Joint Inversion of Rayleigh Wave Group Velocities and Receiver Functions (Dugda et al. 2005) strengthened the idea of lithospheric thinning with crustal and lithospheric thicknesses of 35–44 and 70–80 km beneath the Ethiopian Plateau and 25–35 and 50 km beneath the Main Ethiopian Rift and the Afar. Beneath the East African dome and Lake Turkana, a seismic refraction-wide-angle reflection experiment (Mechie et al. 1997) suggested 35- and 20-km crustal thicknesses, respectively. Similar result also obtained by Rayleigh wave dispersion measurements (Benoit et al. 2006b) that defined an average crustal thickness of 25 ± 5 km for Turkana Depression, some 10–15 km thinner than the crust beneath the Ethiopian and East African plateaus. The lower elevation of Turkana Depression reflect an isostatic response to crustal thinning that is due to the superposition of the multiple phases of rifting in the Mesozoic and Cenozoic (Benoit et al. 2006b).

Basaltic volcanism started in southernmost Ethiopia between 45 and 35 Ma (Davidson and Rex 1980; Ebinger et al. 1993; George et al. 1998) and propagated north and southwards with time (George et al. 1998). It is mainly exposed in the Amaro, Gamo, and Gidole localities in southern Ethiopia where about 1-km thick successions overlay the Late Proterozoic basement and thin layer (~6 m) of Early Tertiary basal sandstone (Zanettine et al.

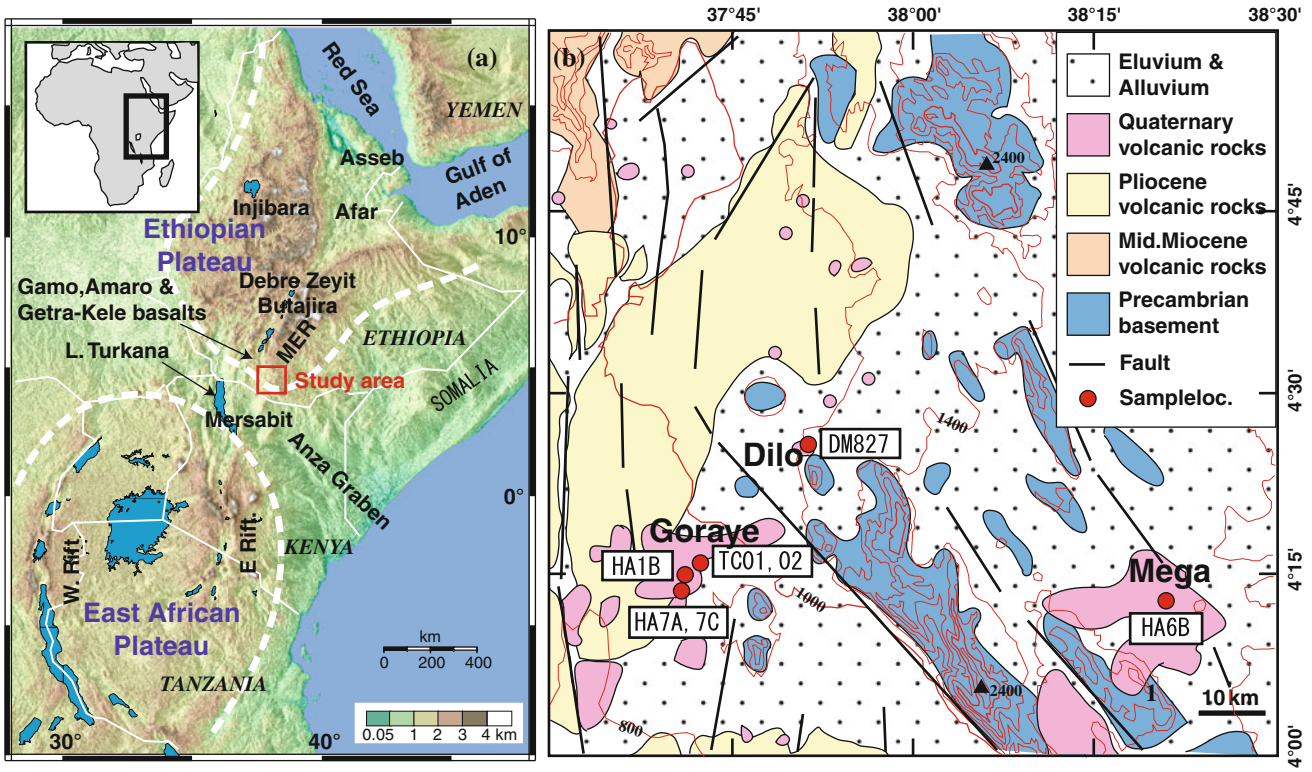

Fig. 1 **a** Shaded relief map (source of data: NASA SRTM30) of East Africa showing tectonic setting of the study region in southern Ethiopia. *MER* main Ethiopian rift, *E* and *W-Rift* Eastern and Western rifts. *Heavy broken lines* (*white*) enclose plateau elevations greater than 1,000 m. The locations of our study site and name of some localities are also indicated. **b** Simplified geological map of the Yabello area showing sample location of mantle xenoliths. Topography is contoured at 200-m intervals

1978; Davidson and Rex 1980; Davidson 1983; Woldegabriel et al. 1991; Ebinger et al. 1993; Stewart and Rogers 1996; George et al. 1998). After the initiations of initial rifting in the southern and central MER (18–15 Ma: WoldeGabriel et al. 1990; Ebinger et al. 2000), widespread episodic syn-rift alkaline basalts and trachytes (19–11 Ma, WoldeGabriel et al. 1990, 1991; Ebinger et al. 1993; Stewart and Rogers 1996; George et al. 1998; George and Rogers 2002; Bonini et al. 2005) occurred in the MER including Getera-Kele locality in southern Ethiopia (Stewart and Rogers 1996). The youngest volcanics in southern Ethiopia were erupted in the Plio-Plistocene and occurred as fissural lavas and cinder cones and are mainly confined to the axial zone of the rift floor along faults (e.g., Yemane et al. 1999). However, Davidson and Rex (1980) reported their occurrence far from the axial zone in the adjacent highlands.

The volcanic activities in Yabello area (southern Ethiopia; Fig. 1b) are characterized by lava flows, spatter, and scoria cones, and maars with pyroclastic deposits and minor phonolites, trachytes and rhyolites that directly lie on the Precambrian crystalline basement. The rocks are alkaline to tholeiitic in composition and their K–Ar dating indicate that they are emplaced in Miocene (12.3–10.5 Ma; alkaline), Pliocene (4.7–3.6 Ma; tholeiite), and Quaternary (1.9–0.3 Ma; alkaline; Fig. 1b, Shinjo et al. 2010). Quaternary alkaline basalts are dominated by basanite and are characterized by porphyritic texture with 7–17% phenocrysts of olivine ($Fo_{79–90}$), clinopyroxene (Mg# = 70–91), and minor opaque minerals within groundmass of olivine ($Fo_{60–83}$), clinopyroxene (Mg# = 66–75), plagioclase, and Fe–Ti oxides (Shinjo et al. 2010).

Petrography of mantle xenoliths from Yabello area

Seven fresh mantle xenoliths hosted in the Quaternary alkaline basalts (Shinjo et al. 2010) are collected from Mega, Dilo, and Goraye localities in Yabello area, southern Ethiopia (Fig. 1b). They are on average about 10 cm in diameter and sub-rounded to angular in shape. On the basis of modal abundance estimated through point counting (2,000 point/thin section), the investigated mantle xenoliths are spinel lherzolites in composition (Fig. 2; Table 1), and they belong to Type I (Frey and Prinz 1978) or Cr-diopside (Wilshire and Shervais 1975) xenoliths. They contain primary assemblages of olivine (44.5–65.2%), orthopyroxene (19.7–36%), clinopyroxene (6.9–17.9%), and spinel

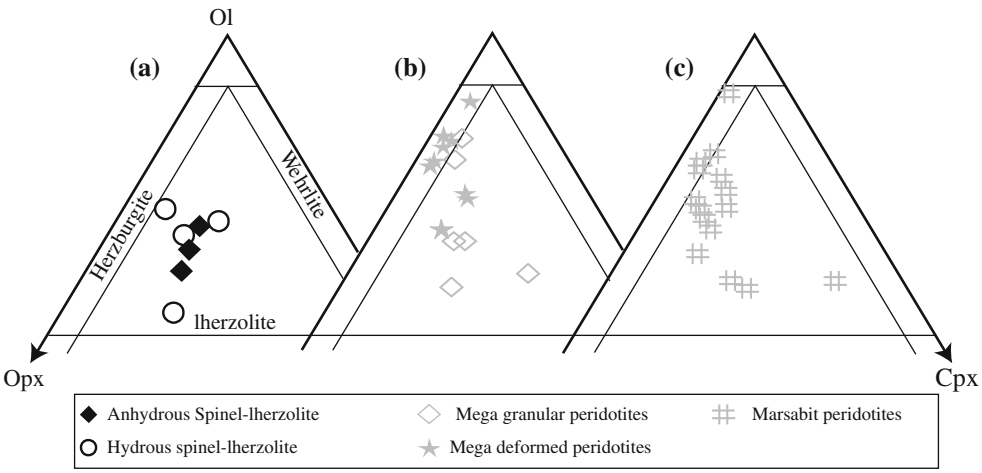

Fig. 2 Plots of modal composition of mantle peridotites from **a** this study, **b** Mega (Bedini et al. 1997; Bedini and Bodinier 1999; Lorand et al. 2003), and **c** Marsabit (Kenya, Kaeser et al. 2006). *Cpx* clinopyroxene, *Ol* olivine, *Opx* orthopyroxene

(0.3–2.9%) with/without amphibole and phlogopite (Table 1). Based on the occurrence of hydrous minerals, the lherzolites are subdivided into two types: anhydrous and hydrous spinel lherzolites (Fig. 3 and Table 1). Trace plagioclase crystals and sulfides as inclusion or interstitial component are also observed in sample DM827. Exsolution lamellae of clinopyroxene in orthopyroxene are common in both types of spinel lherzolites. Some olivine shows kink band with curvilinear grain boundaries. Both hydrous and anhydrous spinel lherzolites are characterized by a protogranular texture (Mercier and Nicolas 1975) with aggregates of coarse-grained (>4 mm in diameter) olivine and pyroxene and fine-grained (sometimes vermicular in shape) spinel crystals (Fig. 3b) and amphibole (Fig. 3d). Sample HA7A contains amphibole-rich vein crosscutting the lherzolites (Fig. 3c). The contact between the spinel lherzolites and the host rock is sharp (Fig. 3a).

Analytical methods

Mineral analyses on seven fresh mantle xenoliths were conducted using energy dispersive X-ray spectrometer (EDX; EDAX Corporation Genesis 4000) attached to scanning electron microscope (SEM; Hitachi 3000 N) at the Department of Physics and Earth Sciences, University of the Ryukyus. EDX operating conditions were 20 kV and 0.5 nA. Mineral constituents were identified from elemental mapping of the whole thin section. Mineral compositions were determined by three point analyses in a given grain for the core part of olivine and pyroxene. Five point analyses for a given grain were done for spinel and amphibole. Average analyses for each mineral are presented in Supplementary Table.

The whole-rock major elements and selected trace elements (Co, Cr, V, Ni, Cu, Zn, Sr, Y, and Zr) were determined on glass beads and pressed powder pellets,

Table 1 XRF analyses of whole-rock major and trace element contents and modal compositions from Yabello peridotite xenoliths, southern Ethiopia

Type	Anhydrous spinel lherzolites			Hydrous spinel lherzolites			
Sample	HA7C	TC01	DM827	HA1B	HA6B	TC02	HA7A
SiO_2 (wt%)	45.68	44.31	45.28	45.71	46.12	46.86	46.25
TiO_2	0.099	0.156	0.125	0.220	0.158	0.206	0.112
Al_2O_3	2.46	4.06	3.40	4.10	4.12	3.30	3.28
Fe_2O_3	8.61	9.63	9.01	8.05	8.72	7.98	9.08
MnO	0.127	0.135	0.124	0.124	0.127	0.120	0.128
MgO	38.13	36.81	37.10	34.92	34.68	35.66	36.10
CaO	3.80	4.10	4.21	5.55	4.93	4.45	3.82
Na_2O	0.208	0.247	0.253	0.360	0.313	0.288	0.292
K_2O	0.015	0.007	0.008	0.028	0.012	0.009	0.044
P_2O_5	0.014	0.014	0.015	0.015	0.014	0.011	0.017
Total	99.14	99.47	99.52	99.07	99.19	98.88	99.12
Zr (ppm)	6	6	6	9	7	8	9
Y	3	4	3	5	4	4	2
Sr	15	14	14	23	15	12	21
Zn	48	62	56	55	52	50	56
Cu	17	18	18	11	15	18	18
Ni	2,261	2,040	2,106	1,906	1,843	1,968	2,068
Co	103	100	100	92	94	95	99
Cr	2,753	2,840	3,463	2,761	2,830	3,527	3,488
V	74	94	82	113	93	89	85
Modal composition (vol. %)							
Ol	61.6	51.2	56.2	61.6	44.5	59.2	65.2
Opx[a]	23.6	30.5	27.1	19.7	36.0	26.7	27.7
Cpx[a]	14.0	15.5	14.6	16.5	17.9	12.4	6.9
Spl	0.8	2.9	2.2	2.2	1.6	1.6	0.3
Amph				tr.	tr.	tr.	tr.
Plag			tr.				
Phl							tr.

Ol Olivine, *Opx* orthopyroxene, *Cpx* clinopyroxene, *Spl* spinel, *Amph* amphibole, *Plag* Plagioclase, *Phl* Phlogopite

[a] Exsolution lamellea; *tr.*, trace. Trace silicate-enclosed and interstitial sulfides in all samples

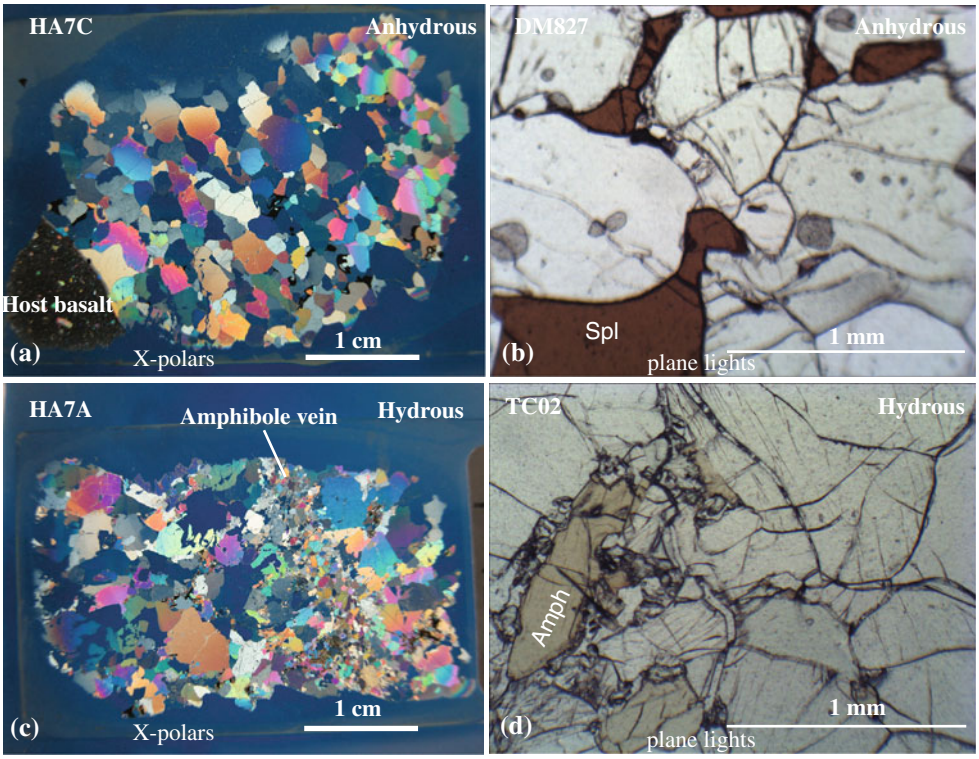

Fig. 3 Selected photomicrographs (cross-polarized and plane light) of spinel lherzolites. **a** anhydrous spinel lherzolite (Sample HA7C) showing sharp contact between host basalt and the lherzolite, **b** anhydrous spinel lherzolite (Sample DM827) showing spinel distribution, **c** hydrous spinel lherzolite (Sample HA7A) having amphibole-rich vein, **d** hydrous spinel lherzolite (Sample TC02) showing amphibole crystal. Both types are characterized by protogranular texture

respectively, by using X-ray fluorescence spectrometry (Shimadzu XRF-1800) at the Department of Physics and Earth Sciences, University of the Ryukyus (Table 1). Calibration curves were constructed using international standard rock samples from the Geological Survey of Japan (GSJ: JA-1, JB-1, and JP-1) and US Geological Survey (USGS: BIR-1, BHVO-2, and DTS-2). Reproducibility and accuracy of the XRF analyses were checked using the international rock standards JB-1, JP-1, and DTS-2 (Imai et al. 1995; Raczek et al. 2001). Based on comparison with the recommended values, accuracy for major elements is estimated to be <1% and those of trace elements <12%.

Further trace element concentrations (including full rare earth element (REE)) for whole-rock, clinopyroxene, and amphibole separates were measured by inductively coupled plasma mass spectroscopy (ICP-MS), Yokogawa Analytical Systems (now Agilent Technologies) HP4500, at the University of the Ryukyus (Table 2). Clinopyroxenes were separated by using an isodynamic magnetic separator while amphibole and larger grains of clinopyroxene were separated by hand-picking under binocular microscope. Clinopyroxene and amphibole separates were leached before being dissolved using 6 M HCl and 2.5 M HCl for 2 h at 110°C, respectively. After rinsed with ultrapure (Milli-Q) water several times, the separates were dissolved in a $HF + HClO_4 + HNO_3$ mixture and placed on hotplate at ~140°C for overnight. The solution was dried down, and $HClO_4$ was added and again placed on hotplate at ~140°C for overnight. After complete evaporation to dryness, the samples were re-dissolved in 6 M HCl and dried down. Then residues were dissolved with 6 M HNO_3 and diluted with Milli-Q to 1% HNO_3 just before final analyses. A GSJ JB-1 standard solution was used as calibration standard, with ^{115}In internal standard. The reproducibility of ICP-MS analyses were checked using the international rock standard BIR-1, JA-1, JP-1, JB-2, and DTS-2. The accuracy of most trace element analyses is within ±5% relative to the recommended values.

Sr, Nd, and Pb isotope analyses of clinopyroxene and amphibole separates were performed on a Finnigan MAT262 mass spectrometer at the University of the Ryukyus, using procedures provided in Shinjo et al. (2000) and Wang et al. (2004), respectively. The isotopic ratios were corrected for mass fractionation by normalizing to $^{86}Sr/^{88}Sr = 0.1194$ and $^{146}Nd/^{144}Nd = 0.7219$. The NIST NBS-987 Sr standard, during this study, gave a mean $^{87}Sr/^{86}Sr = 0.710242 \pm 0.000031$ (2SD; $n = 5$) and the Nd standard La Jolla gave a mean $^{143}Nd/^{144}Nd = 0.511824 \pm 0.000017$ (2SD; $n = 8$). All data for samples were normalized to a value of NBS-987 $^{87}Sr/^{86}Sr = 0.71025$ and La Jolla $^{143}Nd/^{144}Nd = 0.51186$.

^{207}Pb-^{204}Pb double-spiked method was applied to the Pb isotopic analyses. The compositions of fractionation-

Table 2 ICP–MS analyses of whole rock, clinopyroxene and amphibole separates from Yabello peridotite xenolithes, southern Ethiopia

	Anhydrous spinel lherzolites						Hydrous spinel lherzolites								
	HA7C		TC01		DM827		HA1B		HA6B		TC02		HA7A		
	WR	Cpx	WR	Cpx	WR	Cpx	WR	Cpx	WR	Cpx	WR	Cpx	WR	Cpx	Amph
Li (ppm)	1.91	1.70	1.81	1.79	1.78	1.52	2.00	1.52	1.85	1.67	1.66	1.60	1.65	1.45	0.84
Be	0.040	0.097	0.032	0.094	0.028	0.093	0.045	0.130	0.036	0.098	0.030	0.108	0.115	0.304	0.837
Sc	13.9	87.1	15.1	56.7	14.6	53.8	19.2	64.7	15.1	64.1	17.0	72.2	9.5	6.8	51.6
V	58.7	309	75.3	286	68.1	279	93.5	306	80.5	287	76.1	294	70.6	292	352
Cr	1,262	6,605	1,510	3,963	1,676	4,395	1,548	3,463	1,373	3,978	1,750	5,400	1,652	5,682	4,208
Co	108	25.4	109	29.4	108	23.8	96	20.4	99	25.1	99	26.1	105	24	49
Ni	1,999	374	1,830	414	1,877	366	1,700	315	1,678	371	1,733	396	1,825	354	1,030
Rb	0.304	0.025	0.051	0.029	0.032	0.027	0.299	0.037	0.119	0.126	0.060	0.186	0.360	0.072	13.7
Sr	11.87	65.7	9.84	72.8	11.06	81.6	20.21	82.5	12.14	78.9	8.34	54.5	17.44	91	179
Y	2.58	19.0	3.46	22.3	3.08	22.2	5.61	25.9	3.96	24.0	3.83	23.9	2.34	11.3	21.8
Zr	5.33	30.3	6.42	41.0	5.49	39.0	8.82	42.1	6.48	38.7	7.59	48.0	8.20	22.4	436
Nb	0.465	0.120	0.107	0.245	0.077	0.050	0.176	0.118	0.181	0.231	0.038	0.173	2.381	0.792	319
Cs	0.004	0.004	0.000	0.006	0.001	0.006	0.004	0.006	0.002	0.008	0.001	0.008	0.005	0.001	0.18
Ba	3.61	0.147	0.97	0.339	1.08	0.264	5.11	1.099	1.08	1.433	6.40	7.544	2.94	0.687	70.1
La	0.433	0.89	0.121	1.23	0.237	2.02	0.316	1.53	0.186	1.46	0.057	0.59	0.645	4.10	7.23
Ce	0.925	3.33	0.449	4.60	0.381	3.83	0.869	5.19	0.501	3.90	0.255	2.62	1.508	9.81	17.3
Pr	0.131	0.668	0.094	0.950	0.082	0.792	0.176	0.997	0.102	0.807	0.073	0.692	0.203	1.27	2.32
Nd	0.643	4.12	0.617	5.93	0.500	4.85	1.066	6.02	0.641	5.12	0.580	5.31	0.894	5.47	10.29
Sm	0.208	1.70	0.259	2.48	0.208	2.07	0.424	2.42	0.266	2.24	0.296	2.78	0.247	1.54	2.87
Eu	0.087	0.678	0.110	0.964	0.091	0.853	0.177	0.956	0.119	0.942	0.134	1.165	0.097	0.569	0.968
Gd	0.317	2.43	0.400	3.33	0.345	3.15	0.657	3.62	0.447	3.36	0.520	4.18	0.315	1.94	3.34
Tb	0.061	0.466	0.079	0.620	0.070	0.593	0.131	0.692	0.089	0.644	0.099	0.754	0.059	0.354	0.587
Dy	0.418	3.08	0.558	3.97	0.476	3.96	0.909	4.54	0.630	4.23	0.648	4.66	0.394	2.31	3.7
Ho	0.096	0.667	0.124	0.825	0.112	0.88	0.200	0.989	0.146	0.931	0.138	0.958	0.085	0.481	0.746
Er	0.270	1.95	0.374	2.35	0.327	2.45	0.592	2.79	0.437	2.67	0.398	2.54	0.251	1.39	2.12
Tm	0.043	0.288	0.059	0.343	0.053	0.365	0.091	0.413	0.068	0.387	0.059	0.359	0.040	0.201	0.303
Yb	0.295	1.80	0.386	2.09	0.346	2.21	0.593	2.52	0.462	2.36	0.363	2.04	0.263	1.23	1.79
Lu	0.045	0.252	0.061	0.295	0.054	0.307	0.087	0.358	0.068	0.333	0.054	0.287	0.039	0.173	0.248
Hf	0.159	0.97	0.194	1.24	0.168	1.25	0.275	1.36	0.200	1.22	0.242	1.49	0.142	0.648	18.6
Ta	0.027	0.014	0.005	0.022	0.002	0.010	0.005	0.020	0.007	0.023	0.001	0.014	0.071	0.025	26.0
Pb	0.129	0.368	0.033	–	0.040	0.214	0.067	0.283	0.046	0.268	0.040	0.121	0.119	0.457	1.55
Th	0.055	0.014	0.010	0.059	0.015	0.076	0.011	0.077	0.031	0.212	0.002	0.021	0.278	1.19	2.89
U	0.028	0.008	0.014	0.017	0.010	0.051	0.009	0.027	0.047	0.064	0.018	0.016	0.094	0.558	0.777

WR whole rock, *Cpx* clinopyroxene, *Amph* amphibole

corrected values for the NIST NBS-981 Pb standard ($n = 7$) during this study have $^{206}Pb/^{204}Pb = 16.9426 \pm 0.0046$ (2SD), $^{207}Pb/^{204}Pb = 15.4991 \pm 0.0047$ (2SD), and $^{208}Pb/^{204}Pb = 36.7225 \pm 0.0126$ (2SD). The total procedural blank for Sr, Nd, and Pb were <60 pg, <30 pg, and <30 pg, respectively.

Geochemical results

Major element composition of minerals

Olivine

Olivines are dominantly forestrite ($Fo_{89–91}$), whose compositions are within the range of Mega granular peridotite ($Fo_{89–92}$, Lorand et al. 2003), primitive mantle olivine ($Fo_{86–90}$: Glücklich and Mercier 1989; Chen et al. 2003), and Type I xenoliths ($Fo_{86–91}$: Frey and Prinz 1978). There is no major compositional difference between hydrous and anhydrous spinel lherzolites. NiO content ranges from 0.31 to 0.41 (Supplementary Table) comparable to Type I xenoliths (0.30–0.54: Frey and Prinz 1978). NiO contents of this study broadly overlap (Fig. 4a) with peridotite xenoliths from the surrounding region (Conticelli et al. 1999; Kaeser et al. 2006; Ferrando et al. 2008; Teklay et al. 2010). Except for sample HA7A that has amphibole-rich vein, the plot of Fo contents of olivine against its modal proportions (Fig. 4b) displays subtle increase in Fo with increasing modal olivine along the oceanic trend defined by Boyd (1989).

Clinopyroxene

Clinopyroxenes (Cpx) are dominantly Cr-diopside ($Wo_{44.2–48.6}En_{46.8–49.8}Fs_{4.5–6.5}$) with Mg# (100 Mg/(Mg + Fe)) varying from 90 to 91.7 for hydrous and from 88.4 to 91.5 for anhydrous spinel lherzolites. Cr_2O_3 ranges 0.64–0.94 wt%, Al_2O_3 5.18–6.67 wt%, and TiO_2 0.18–0.90 wt%, respectively (Supplementary Table). The Al_2O_3 contents fall within the field of worldwide spinel peridotites (Fig. 4d; Rudnick et al. 1993).

Orthopyroxene

Orthopyroxenes are dominantly enstatites ($Wo_{0.7–1.7}En_{88.3–89.2}Fs_{9.7–11.7}$) with Mg# varying from 88.1 to 90.3. They have 3.39–4.50 wt% Al_2O_3, 0.07–0.25 wt% TiO_2, 0.27–0.58 wt% Cr_2O_3, and 0.26–0.45 wt% Na_2O (Supplementary Table), but they are characterized by relatively higher TiO_2 and Na_2O contents than the previously published data for peridotite xenoliths in the surrounding regions (0.01–0.16 wt% TiO_2, 0.02–0.16 Na_2O wt%, Conticelli et al. 1999; Kaeser et al. 2006; Ferrando et al. 2008).

Spinel

Spinels are characterized by limited Cr# (Cr/(Cr + Al)) from 0.06 to 0.12 (Supplementary Table) within the range of Type I xenoliths (0.08–0.58: Frey and Prinz 1978). They are aluminous spinel with 59.01–64.43 wt% Al_2O_3, 6.29–11.65 wt% Cr_2O_3, and 0.13–0.31 wt% TiO_2 (Supplementary Table). As shown in Fig. 4c, spinel and coexisting olivine composition plotted in the field of fertile spinel peridotites (Cr# < 0.2) within the olivine spinel mantle array (OSMA) indicating subtle partial melting and melt extraction processes in the spinel stability field (Arai 1994).

Amphibole and phlogopite

The amphibole is dominantly pargasite (after Leake et al. 1997) with Mg# ranging between 52.2 and 89.9 (Supplementary Table). It shows relatively low and limited variations of K_2O (0.42–2.17 wt%) and TiO_2 (0.63–2.97 wt%) with higher CaO (8.03–11.4 wt%) and Al_2O_3 (15.33–19.70 wt%). The spinel lherzolites (HA7A) also contain phlogopite with 0.05 wt% CaO, 1.15 wt% TiO_2, and 13.50 wt% K_2O (Supplementary Table).

Plagioclase and Fe–Ni sulfide

Only sample DM827 contains trace amount of plagioclase and Fe–Ni sulfide (Table 1 and Supplementary Table). The plagioclase has high albite content ($Ab_{58}An_{42}$) with 8.76 wt% CaO, 6.69 wt% Na_2O, 26.99 wt% Al_2O_3, and 57.14 wt% SiO_2. Two spot analyses on the same sample show that Fe–Ni sulfide contains 11.31–28.78 wt% FeO and 14.99–35.5 wt% NiO with 3.95 wt% CuO and 56.22 wt% SO_3 (Supplementary Table).

Whole-rock major element compositions

Whole-rock chemistry of the spinel lherzolites shows restricted ranges of major oxides with MgO contents varying from 34.7 to 38.1 wt% (Table 1). Selected oxides were plotted against MgO together with, for comparison, the compositions of continental (McDonough 1990; Maaløe and Aoki 1977), average abyssal (Boyd 1989), southern Ethiopia (Mega, Bedini et al. 1997; Mega-Megado, Conticelli et al. 1999), northwestern Ethiopia (Injibara-Meráwi, Conticelli et al. 1999), and Assab (Teklay et al. 2010) peridotites (Fig. 5). They are characterized by high SiO_2 (44.3–46.9 wt%) and Fe_2O_3 (7.98–9.63 wt%) contents. CaO, Al_2O_3, and TiO_2 are negatively correlated with MgO along the regression line defined by Maaløe and Aoki (1977) for world-wide spinel peridotites. The lherzolites from this study display fertile

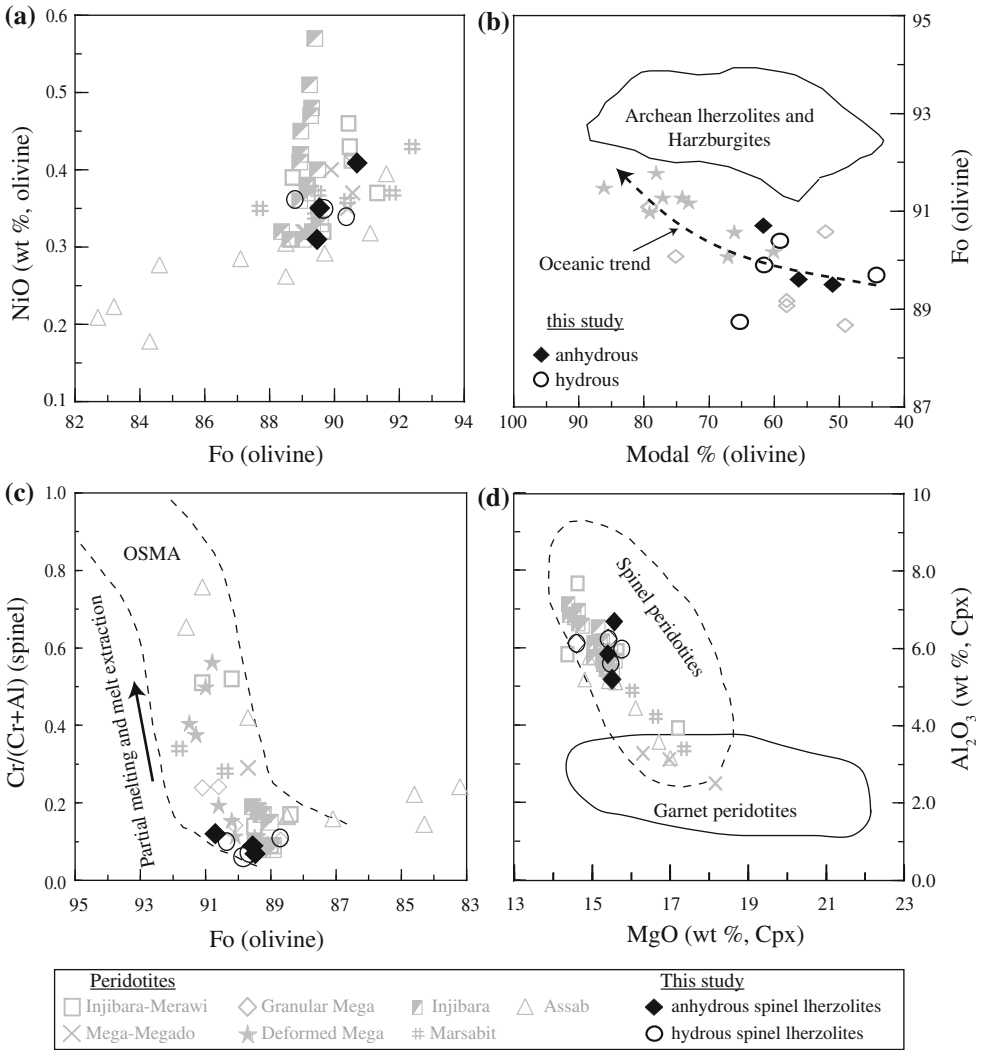

Fig. 4 Plots of selected mineral composition of spinel lherzolites from this study, compared with the surrounding regions. **a** Fo content vs. NiO (wt%) of olivine, **b** Modal % vs. Fo content of olivine, **c** Fo content and Cr/(Cr + Al) of coexisting olivine and spinel, and **d** MgO vs. Al_2O_3 (wt%) of clinopyroxene. Data from Injibara-Meráwi and Mega-Megado (Conticelli et al. 1999), Mega (Bedini et al. 1997; Lorand et al. 2003), Injibara (Ferrando et al. 2008), Mersabit (Kenya, Kaeser et al. 2006) and Assab (Eritrea, Teklay et al. 2010) are also shown. The olivine-spinel mantle array (OSMA) is from Arai (1994). Oceanic trend and field of Archean lherzolites and harzburgites are from Boyd (1989) and Boyd et al. (1997). Fields for worldwide spinel and garnet peridotites are from Rudnick et al. (1993)

compositions analogous to primitive mantle (Jagoutz et al. 1979; Hart and Zindler 1986; Hirose and Kushiro 1993; Baker and Stolper 1994; McDonough and Sun 1995). Their CaO/Al_2O_3 ratios vary from 1.01 to 1.55, higher than the value of primitive mantle (0.79–0.96; Fig. 5d).

Trace element compositions for minerals and whole rock

Cpx and amphibole separates and whole-rock trace element analyses from spinel lherzolites are given in Table 2 and shown in Fig. 6. Also plotted, for comparison, are host alkali basalts (Fig. 6e and f; Shinjo et al. 2010) and REE abundances of Cpx from Mega peridotites (Fig. 6a and c; Bedini et al. 1997; Bedini and Bodinier 1999). Cpx of both anhydrous and hydrous spinel lherzolites display similar chondrite-normalized REE pattern but have higher REE abundances than their corresponding whole-rock compositions (Fig. 6a and c). REE abundances for whole rock and Cpx show almost flat middle to heavy REE patterns ($(Dy/Yb)_{n,wr} = 0.92–1.19$; $(Dy/Yb)_{n,cpx} = 1.15–1.53$) with slightly depleted light REE ($(La/Yb)_{n,wr} = 0.11–1.05$; $(La/Yb)_{n,cpx} = 0.21–0.67$) patterns. LREE depletion is highly pronounced in both Cpx and whole rock of sample TC02 from hydrous type (Fig. 6c). Sample DM827 displays negative Ce anomaly on both Cpx separate and whole rock, while sample HA7C shows slight enrichment of LREE on whole rock (Fig. 6a). Excluding Cpx from sample HA7A, Cpx in the other spinel lherzolites from this study displays similar patterns as Cpx in granular peridotite xenoliths from Mega ($(La/Yb)_{n,cpx} = 0.09–0.7$; Fig. 6c). They are unlike Cpx in Mega-deformed peridotites ($(La/Yb)_{n,cpx} = 1.6–11$; Fig. 6a; Bedini et al. 1997). Sample (HA7A) that has amphibole-rich vein shows marked LREE enrichment relative to HREE for whole rock ($(La/Yb)_{n,wr} = 1.76$; $(Dy/Yb)_{n,wr} = 1$), amphibole

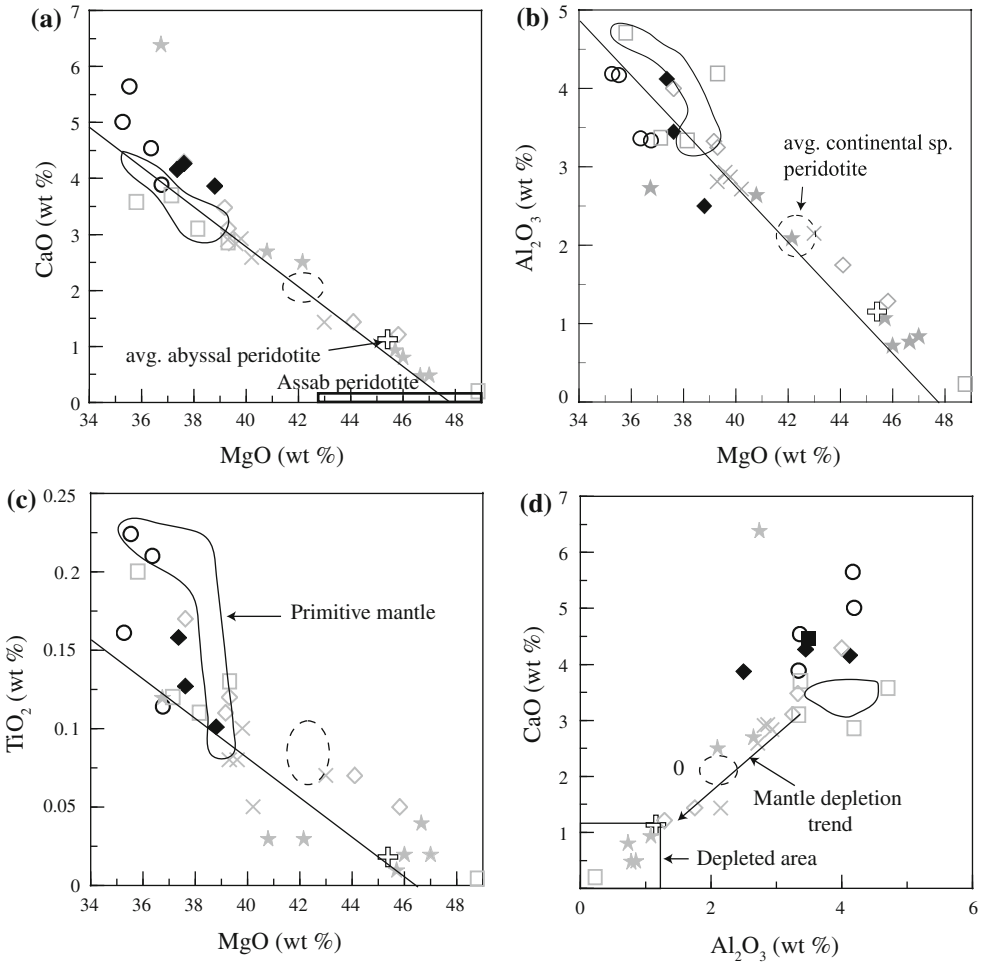

Fig. 5 Plots of selected whole-rock major element composition (wt%) of spinel lherzolites MgO vs. **a** CaO, **b** Al_2O_3, **c** TiO_2, and **d** CaO vs. Al_2O_3, compared with continental (McDonough 1990; Maaløe and Aoki 1977), average abyssal (Boyd 1989) peridotites and peridotites from the surrounding region. Compositions of primitive mantle are from Jagoutz et al. (1979), Hart and Zindler (1986), Hirose and Kushiro (1993), Baker and Stolper (1994), and McDonough and Sun (1995). Regression line is from Maaløe and Aoki (1977). Depleted area is from Boyd (1989). Data sources and *symbols* are as in Fig. 4

$((La/Yb)_{n,amph} = 2.88$; $(Dy/Yb)_{n,amph} = 1.38)$, and clinopyroxene $((La/Yb)_{n,cpx} = 2.39$; $(Dy/Yb)_{n,cpx} = 1.26$; Fig. 6e). Primitive mantle-normalized incompatible trace element patterns of Cpx with the exception of Rb, Ba, Nb, Ta, display enriched abundances than the whole-rock compositions (Fig. 6b, d). Most of the whole rock and Cpx separate of the same sample in anhydrous and hydrous spinel lherzolites are variably depleted LILE (Rb, Ba, and Th) and LREE with distinct negative anomalies of Nb and Ta and only subtle Ti negative anomaly in Cpx separates (Fig. 6b and d). The whole rocks and Cpx separates are characterized by variable ratios of highly incompatible elements, Ba/Nb (6–168.4, 1.2–43.6), Ba/Th (34.8–3,200, 0.6–359.2), Zr/Nb (11.5–199.7, 28.3–277.5), and La/Nb (0.27–3.08, 3.41–40.40). The exception is whole-rock incompatible element abundance of sample HA7C, which has flat primitive mantle-normalized pattern with slight U and Pb-positive anomalies and characterized by the absence of Nb and Ta negative anomalies. The anhydrous spinel lherzolites mainly contain highly depleted Rb and Ba than the hydrous one, but whole-rock hydrous spinel lherzolites have more depleted in Th. In sample HA7A that has amphibole-rich vein, the amphibole separate shows REE and primitive mantle-normalized patterns enrich in LREE and positive Nb–Ta and Zr–Hf anomalies. In contrast, its Cpx shows enrich in LREE but depleted Rb and Ba with Nb–Ta and subtle Zr–Hf–Ti negative anomalies (Fig. 6f).

Sr–Nd–Pb isotope compositions of clinopyroxene and amphibole separates

The Sr–Nd–Pb isotope ratios of Cpx and amphibole separates from the spinel lherzolites are given in Table 3 and illustrated in Fig. 7. Cpx from the spinel lherzolites have a limited range of $^{87}Sr/^{86}Sr$ from 0.701796 to 0.702945 and $^{143}Nd/^{144}Nd$ from 0.513029 to 0.513478, respectively. In contrast, the amphibole from sample HA7A, which has amphibole-rich vein, has higher $^{87}Sr/^{86}Sr$ (0.703019) and lower $^{143}Nd/^{144}Nd$ (0.512992) than the Cpx. The $^{87}Sr/^{86}Sr$ and $^{143}Nd/^{144}Nd$ of the host basalts are 0.703081–0.703365 and 0.512839–0.512901 (Shinjo et al. 2010; Fig. 7a),

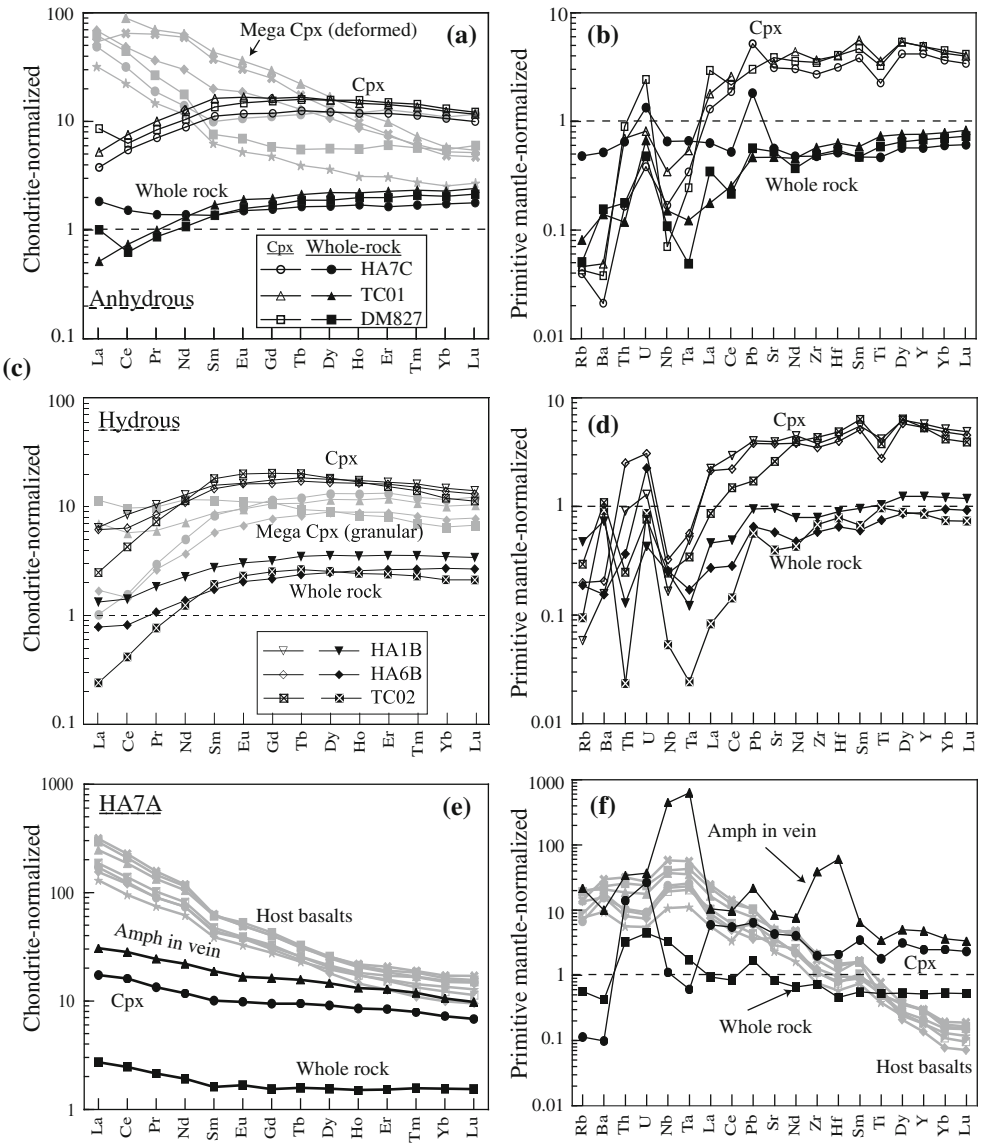

Fig. 6 Chondrite-normalized REE and primitive mantle-normalized multielement patterns for clinopyroxene separates and whole rocks. **a** REE patterns for anhydrous spinel lherzolites, **b** multielement patterns for anhydrous spinel lherzolites, **c** REE patterns for hydrous spinel lherzolites, **d** multielement patterns for hydrous spinel lherzolites and **e** REE for amphibole separate form sample HA7A, and **f** multielement for amphibole separate form sample HA7A, compared with Mega clinopyroxene separates (Bedini et al. 1997; Bedini and Bodinier 1999) and host alkaline basalts (Shinjo et al. 2010). Chondrite and primitive mantle values are from Sun and McDonough (1989)

respectively, and plotted together with the fields of Mesozoic to Quaternary plume-related basalts from Djibouti (Deniel et al. 1994), MER (Furman et al. 2006a), southern Ethiopia (George and Rogers 2002), and Turkana Depression (Furman et al. 2004, 2006b). Thus, those values are more enriched than the Cpx and amphibole separates from the peridotite xenoliths. For comparison, the isotopic data for peridotites from Saudi Arabia (Blusztajn et al. 1995), Yemen (Baker et al. 1998), Jordan (Shaw et al. 2007), and Assab (Teklay et al. 2010) are also plotted in Fig. 7a. All the data are clustering within the Arabian lithospheric mantle field (Baker et al. 1998).

The Cpx have wide range of $^{206}Pb/^{204}Pb$ (17.8601–19.6803), $^{207}Pb/^{204}Pb$ (15.4343–15.6385), and $^{208}Pb/^{204}Pb$ (37.3780–39.4649). The amphibole from sample HA7A, which has amphibole-rich vein, has $^{206}Pb/^{204}Pb$ of 19.4178, $^{207}Pb/^{204}Pb$ of 15.5946, and $^{208}Pb/^{204}Pb$ of 39.3330. Variations in Pb isotopic ratios (Fig. 7c, d) define a linear trend parallel to the Northern Hemisphere Reference Line (NHRL) of Hart (1984). The variations are extending between DMM and the field of the host alkaline basalts (Shinjo et al. 2010) and other Mesozoic to Quaternary plume-related basalts from Djibouti (Deniel et al. 1994), MER (Furman et al. 2006a), southern Ethiopia (George and Rogers 2002), and Turkana Depression (Furman et al. 2004, 2006b). The Cpx isotopic data from this study overlap the range of Jordan (Shaw et al. 2007) and Yemen (Baker et al. 1998) peridotites (Fig. 7). $^{206}Pb/^{204}Pb$ is broadly correlated with $^{87}Sr/^{86}Sr$ and $^{143}Nd/^{144}Nd$ values, and the data are also clustered between DMM and the field of the host alkaline and other plume-related basalts (Fig. 7e, f).

Table 3 Sr, Nd, and Pb isotopic data for clinopyroxene (Cpx) and amphibole (Amph) separates from Yabello peridotite xenoliths, southern Ethiopia

Sample	Mineral	$^{87}Sr/^{86}Sr$	$^{143}Nd/^{144}Nd$	Sm	Nd	$^{147}Sm/^{144}Nd$	ε_{Nd}	T_{DM} (Ga)	$^{206}Pb/^{204}Pb$	$^{207}Pb/^{204}Pb$	$^{208}Pb/^{204}Pb$
Anhydrous spinel lherzolites											
HA7C	Cpx	0.702712 (16)	0.513170 (9)	1.700	4.120	0.2492	10.37	0.23	18.7047	15.5336	38.5724
TC01	Cpx	0.702016 (14)	0.513333 (9)	2.480	5.930	0.2526	13.55	0.83	17.8601	15.4343	37.3780
DM827	Cpx	0.702070 (14)	0.513394 (10)	2.070	4.850	0.2578	14.74	0.94	18.6771	15.5200	38.6785
Hydrous spinel lherzolites											
HA1B	Cpx	0.702875 (17)	0.513125 (8)	2.420	6.020	0.2428	9.49	0.05	18.1180	15.4961	37.8623
HA6B	Cpx	0.701796 (16)	0.513478 (18)	2.240	5.120	0.2643	16.38	1.07	18.2479	15.4374	38.1340
TC02	Cpx	0.702510 (14)		2.780	5.310	0.3162			19.6803	15.6385	39.4649
HA7A	Cpx	0.702945 (14)	0.513029 (18)	1.540	5.470	0.1700	7.62	0.31	19.4267	15.5991	39.3483
	Amph	0.703019 (15)	0.512992 (16)	2.870	10.290	0.1685	7.60	0.30	19.4178	15.5946	39.3330

Number in parentheses denote 2SE (standard error) corresponding to last significant digits; ε_{Nd} calculated according to DePaolo and Wasserburg (1976), with present-day $^{143}Nd/^{144}Nd_{CHUR} = 0.512638$ (Jacobsen and Wasserburg 1980). T_{DM} calculated according to the depleted mantle model of Goldstein et al. (1984), using $^{147}Sm/^{144}Nd_{DM} = 0.2124$, $^{143}Nd/^{144}Nd_{DM} = 0.513114$ (Michard et al. 1985) and $\lambda 147Sm = 6.54 \times 10^{-12}$ year^{-1}

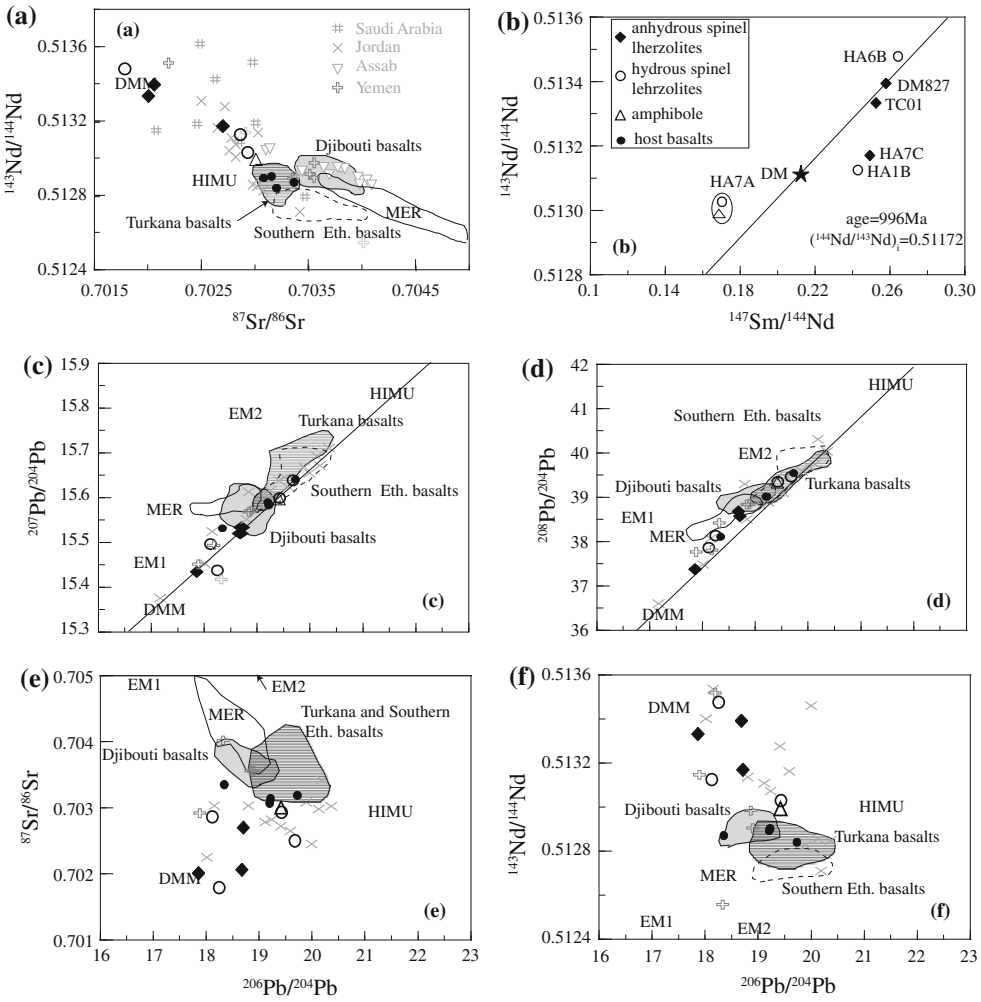

Fig. 7 Plots of **a** $^{87}Sr/^{86}Sr$ vs. $^{143}Nd/^{144}Nd$, **b** $^{147}Sm/^{144}Nd$ vs. $^{143}Nd/^{144}Nd$, $^{206}Pb/^{204}Pb$ vs. **c** $^{207}Pb/^{204}Pb$, **d** $^{208}Pb/^{204}Pb$, **e** $^{87}Sr/^{86}Sr$, and **f** $^{143}Nd/^{144}Nd$ for clinopyroxene and amphibole separates from spinel lherzolites compared with isotopic composition of Saudi Arabia (Blusztajn et al. 1995), Yemen (Baker et al. 1998), Jordan (Shaw et al. 2007), Assab (Teklay et al. 2010) peridotites and Host basalt (Shinjo et al. 2010), Djibouti recent basalts (<4 Ma, Deniel et al. 1994), MER Quaternary basalts (Furman et al. 2006b), Southern Ethiopia Miocene basalts (George and Rogers 2002), and Turkana Quaternary and Mesozoic basalts (Furman et al. 2004; 2006a). Ideal mantle end members are from Zindler and Hart (1986)

As shown in Fig. 7a–f, the isotopic data extends from depleted end member (DMM; Zindler and Hart 1986) to enriched component that has isotopic compositions similar to the host alkaline basalts (Shinjo et al. 2010) and other plume-related basalts (Deniel et al. 1994; George and Rogers 2002; Furman et al. 2004, 2006a, b).

Discussions

Partial melting and melt extraction

Both types of spinel lherzolites have whole-rock basaltic component (CaO = 3.80–5.55 wt%, Al_2O_3 = 2.46–4.12 wt%, and MgO = 34.7–38.1 wt%) analogous to the composition of primitive mantle (Jagoutz et al. 1979; Hart and Zindler 1986; Hirose and Kushiro 1993; Baker and Stolper 1994; McDonough and Sun 1995). In addition, the compositions of spinel (Cr# = 0.062–0.117 and Al_2O_3 = 59.01–64.43 wt%) and clinopyroxene (Mg# = 88.4–91.7, Al_2O_3 = 5.18–6.67 wt% and TiO_2 = 0.49–0.90) indicate that the spinel lherzolites represent fertile upper mantle, which have not experienced significant partial melting and melt extraction processes. The relationships of spinel Cr# and the coexisting olivine Fo contents show no significant variations of spinel Cr# related to progressive partial melting, rather the data cluster in the primitive mantle field (Fig. 4c). As shown in Fig. 4b, the spinel lherzolites of this study including Mega granular lherzolites (Bedini et al. 1997) show subtle effect of progressive depletion by partial melting, and they are significantly differ from the depleted Archean lithospheric mantle (Boyd 1989; Boyd et al. 1997), implying that no depleted Archean lithosphere has been sampled in the area. It is also noted that, as expected from the extraction of basaltic partial melts, the correlations of clinopyroxene (Al_2O_3) and coexisting spinel (Al_2O_3 and Cr_2O_3) do not show any increase in Cr_2O_3/Al_2O_3 value with decreasing Al_2O_3 (figure not shown) as illustrated for depleted Mt. Shadwell spinel lherzolites (Norman 1998). Since CaO and Al_2O_3 are removed when peridotite partially melts and are not added by metasomatic effect (Stern and Johnson 2010), they can be good tracer of the degree of depletion by melt extraction. As shown in Fig. 5d, all samples of the lherzolites from this study show high CaO than the primitive mantle composition, suggesting that there is no depletion in basaltic component by partial melting effects.

However, the slightly depleted LREE in the chondrite-normalized REE patterns of the Cpx and whole rock provide evidence for subtle partial melting event in these xenoliths, which selectively removed LREE from the mantle relative to MREE and HREE (Fig. 6a, c). In Fig. 8a and b, REE contents of whole rocks are compared with residual melt compositions of primitive mantle source after fractional and batch melting; the flat MREE and HREE of whole-rock analyses of both hydrous and anhydrous lherzoliths can be produced by <10% batch and ≤5 fractional melting of primitive mantle (Sun and McDonough 1989). The degree of partial melting of anhydrous spinel lherzolites is higher than that of hydrous spinel lherzolites. However, the enrichment of some trace elements observed in the spinel lherzolites from Turkana Depression cannot be explained by partial melting processes alone but strongly requires activity of metasomatism due to melt (or fluid) infiltration from the host rock.

Effects of metasomatism

In both hydrous and anhydrous spinel lherzolites of this study, whole-rock and mineral (Cpx and amphibole) compositions indicate modal and cryptic metasomatic (Dawson 1984) enrichments as recorded through mineralogical change (amphibole and phlogopite, hydrous spinel lherzolites) or compositional enrichments without any involvement of new minerals (anhydrous spinel lherzolites), respectively.

The Cpx from both hydrous and anhydrous spinel lherzolites display similar types of REE and incompatible element patterns but with enriched abundance than the chondrite (C1) and primitive mantle compositions (Sun and McDonough 1989; Fig. 6a–d). Exceptions are variable depletion in some LREE, LILE (Ba and Rb), and HFSE (Nb, Ta, Th, and U) than primitive mantle compositions, which also highly differs from the enriched host alkaline basalts (Fig. 6). Nb and Ta are strongly depleted in Cpx and whole rock in both hydrous and anhydrous spinel lherzolites. But the degree of depletion varies between the two type lherzolites.

As shown in Fig. 6f (sample HA7A), the contents of Nb, Ta, Zr, and Hf are much higher in amphibole from amphibole vein than in the coexisting Cpx, suggesting that Nb, Ta, Zr, and Hf are partitioned strongly into amphibole during metasomatic enrichments. Hence, the amphibole vein from the initially percolated hydrous fluid/melt has Nb–Ta positive anomalies and caused Nb–Ta depletion in the residual fluid/melt as discussed in Ionov and Hofmann (1995). We infer that further percolation of the residual fluid/melt after the formation of amphibole vein and reaction with the peridotite can induce formation of disseminated hydrous minerals in hydrous spinel lherzolite, and the metasomatized peridotite became depleted in Nb and Ta (Fig. 6b, d). Despite of presence or absence of hydrous phase, both hydrous and anhydrous spinel lherzolites have the same trace element patterns (Fig. 6a–d). We infer that the indistinguishable trace element characteristics between hydrous and anhydrous lherzolites are mainly due to very small amount of hydrous minerals (<1 vol%) in hydrous lherzolites compared to Cpx (Table 1). Thus, they do not contribute significantly to REE budget of hydrous spinel lherzolites. Cpx is therefore the main carrier of REE, Ti, Sr, and Zr among the common phases of spinel peridotites in hydrous and anhydrous spinel lherzolites.

The amphibole vein and disseminated hydrous phase (amphibole and phlogopite) indicate that the spinel

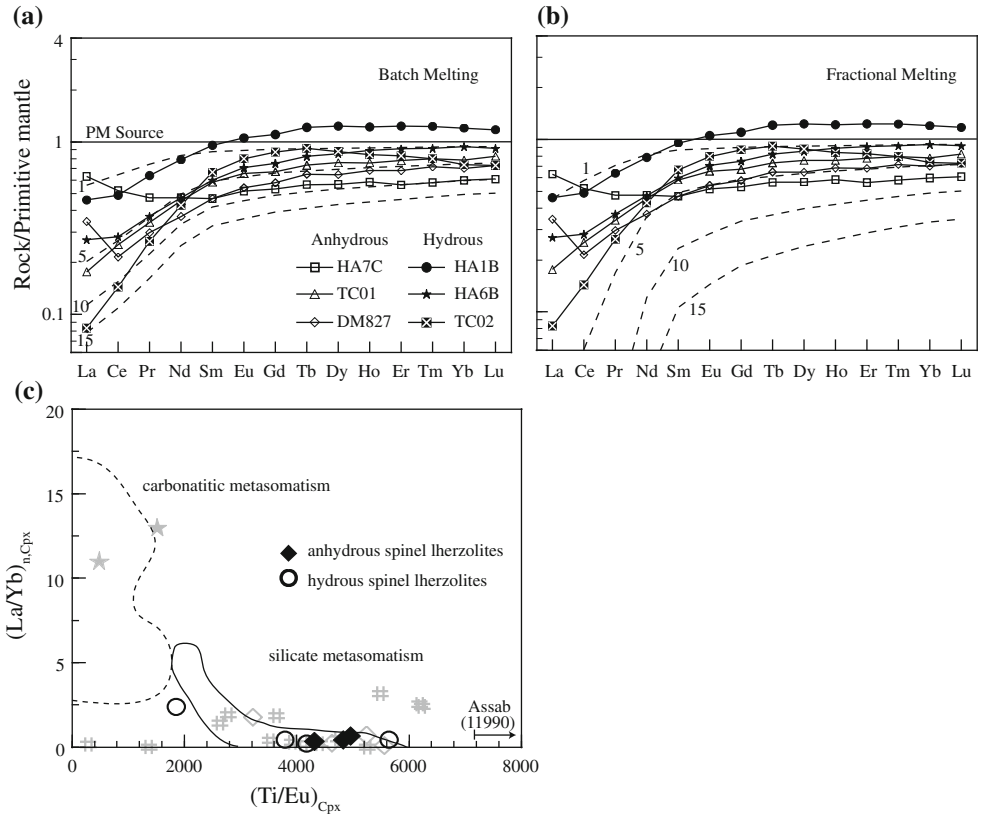

Fig. 8 Plot of **a** and **b** comparison of model melt by batch and fractional melting, and **c** Ti/Eu vs. $(La/Yb)_n$ for clinopyroxenes in the spinel peridotites compared with Mega (Bedini et al. 1997), Assab (Eritrea, Teklay et al. 2010), and Marsabit (Kenya, Kaeser et al. 2006) peridotites. Distribution coefficients and primitive mantle mineralogy are from Niu and Hékinian (1997) and Baker and Stolper (1994). Primitive mantle values are from Sun and McDonough (1989). Carbonatitic and silicate metasomatism fields are from Coltorti et al. (1999)

lherzolites have been metasomatized by hydrous fluid infiltrated the lithosphere possibly during the early stage of plume rising (Ferrando et al. 2008). It is worth mentioning that the influx of carbonatitic melts and hydrous fluids from the Afar plume is thought to be the source of the amphibole (±apatite) in the spinel lherzolites from Yemen (Baker et al. 1998). Besides, Bedini et al. (1997) considered percolating basaltic and carbonatite melts as metasomatic agent for granular and deformed peridotites, respectively, from Mega area, southern Ethiopia. However, hydrous and anhydrous spinel lherzolites in the present study are characterized by the lack of significant LREE enrichment, low LILE abundances, the absence of strong Ti–Zr–Hf negative anomaly, and low La/Yb and high Ti/Eu, implying that the spinel lherzolites from Turkana Depression have not been significantly metasomatized by carbonatite melt/fluid (Shinjo and Matsumura 2006).

As shown in the metasomatism discriminative diagram (Fig. 8c), both types of spinel lherzolites from this study have high Ti/Eu and low $(La/Yb)_n$, implying that the metasomatic agent was silica-rich melt (or fluid) rather than carbonate-rich fluid (Coltorti et al. 1999), possibly related to the emplacement of asthenospheric mantle plume (Ferrando et al. 2008). Similarly, a single metasomatic event caused by such a silicate melt infiltration is also proposed for peridotite xenoliths from central MER (Rooney et al. 2005). Thus, we suggest that the metasomatic agents for Turkana lherzolites have combined characteristics of hydrous fluid and silicate melt.

Moreover, the progressive variations of Sr, Nd, and Pb isotopic compositions (Fig. 7) toward the enriched host basalts also suggest the effect of silicate metasomatism. The most metasomatized lherzolites plot closer to the enriched (HIMU affinity) composition of host basalt and other plume-related basalts from the region suggesting a sublithospheric source with high-μ (HIMU) Sr–Nd–Pb isotopic affinities (Fig. 7). Though hydrous and anhydrous spinel lherzolites differently metasomatized, the similarity in their isotopic composition suggests that the metasomatic agents were derived from the same source region. Thus, the metasomatism of subcontinental lithospheric mantle beneath Turkana Depression could be associated with hydrous fluid and silicate melt infiltration from sublithospheric source with high-μ (HIMU) Sr–Nd–Pb isotopic affinities similar to the proposed Kenyan plume composition (Rogers et al. 2000) or from the secondary plumes (plumelets) that are proposed to contain lenses of HIMU-like composition within the broad mantle upwelling zone connected to the African superplume (Meshesha and Shinjo 2008 and references therein).

Table 4 P–T estimates for Yabello peridotite xenoliths, southern Ethiopia

Sample	Temperature (°C)		Pressure (kb)	
	$T_{Ca–Opx}$	$T_{Cr–Al–Opx}$	$T_{Two–Px}$	P_{En}
Anhydrous spinel lherzolites				
HA7C	914	875	934	17.9
TC01	1,052	938	1,031	22.2
DM827	904	986	984	12.8
Hydrous spinel lherzolites				
HA1B	847	876	899	15.6
HA6B	958	910	987	19.8
TC02	934	897	1,001	18.4
HA7A	940	867	968	19.1

$T_{Ca–Opx}$ = Ca in Opx thermometer of Brey and Köhler (1990); $T_{Cr–Al–Opx}$ = Cr–Al–Opx thermometer of Witt-Eickschen and Seck (1991); $T_{Two–Px}$ = Two pyroxene thermometer of Wells (1977); P_{En} = Enstatite barometers of Mercier (1980)

Temperature and pressure estimates

The equilibration temperature and pressure estimations of the spinel lherzolites are reported in Table 4. The absence of any mineral reaction rims and their protogranular (primary) texture of both types of spinel lherzolites indicate that the minerals were in equilibrium before eruption. Therefore, the coexisting anhydrous minerals can be used to estimate the equilibrium temperature and pressure. The temperature estimations were done using Wells (1977), Brey and Köhler (1990) and Witt-Eickschen and Seck (1991) geothermometers. Since temperature estimates of Brey and Köhler (1990) require an estimate of pressure, the estimations were done based on temperature-independent Mercier (1980) barometer (Table 4). The two-pyroxene (Wells 1977) temperature estimates for spinel lherzolites in this study give a temperature ranging from 899 to 1,031°C. Ca content in orthopyroxene (Brey and Köhler 1990) gives a slightly wider range of temperature (847–1,052°C). Further temperature constraints from the Al and Cr contents of orthopyroxene (Witt-Eickschen and Seck 1991) give temperature estimates ranging from 867–986°C that is within the calculated range of Brey and Köhler (1990) and Wells (1977) geothermometer (Table 4). The estimated temperature values of the studied spinel lherzolites using the different thermometers are comparable to the range of previous temperature estimates for mantle peridotites from southern Ethiopia (850–1,040°C (Mega), Bedini et al. 1997; 878–1034°C (Mega-Meráwi), Conticelli et al. 1999), northwestern Ethiopia (947–1,015°C (Injibara), Ferrando et al. 2008; 875–990°C (Injibara-Meráwi), Conticelli et al. 1999), and Assab (870–1,031°C, Teklay et al. 2010) areas. The pressure estimates were done using temperature-independent single-pyroxene barometer of Mercier (1980),

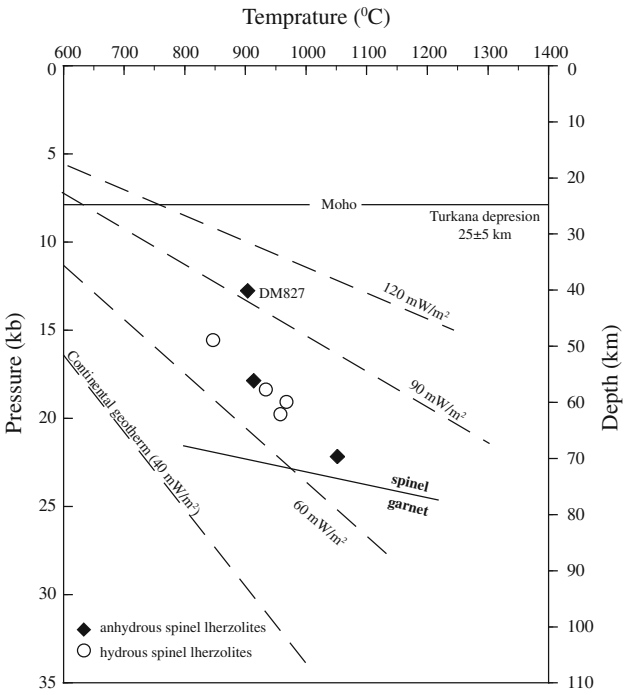

Fig. 9 P–T plot for the spinel lherzolites. The crust thickness is 25 ± 5 km Turkana Depression (Benoit et al. 2006a). Geothermal gradient is based on 40, 60, 90, and 120 mW/m^2 heat flow (Pollack and Chapman 1977). Spinel and garnet transition is from Köhler and Brey (1990)

which gives a wider range of equilibrating pressure from 12.8 to 22.2 kb for enstatites before incorporated into the ascending host magma (Table 4). DM827 is the only one sample that gives lower pressure estimate (12.8 kb). The coexisting of plagioclase and spinel in this sample DM827 suggests that it is from the transition zone of spinel-plagioclase stability field. It must be brought to the pressure that was stable for plagioclase to coexist with spinel. The pressure range for the majority of spinel lherzolites (15.6–22.2 kb) obtained in this study is in a good agreement to the stability field of spinel peridotites. It is higher than the previously estimated pressure range for Mega-Megado (6.7–13 kb, Conticelli et al. 1999) and Injibara-Meráwi (10.1–13.9 kb, Conticelli et al. 1999) but comparable with Injibara (13–20 kb, Ferrando et al. 2008) and Assab (8–20 kb, Teklay et al. 2010) mantle peridotites.

As shown in Fig. 9, to estimate the extraction depths of the spinel lherzolites, Brey and Köhler (1990) geothermometer and Mercier (1980) geobarometer were applied. The spinel lherzolites of Turkana Depression are therefore determined to be derived from 50 to 70 km depth corresponding to the upper mantle in the stability field of spinel (e.g., Wyllie 1981; Köhler and Brey 1990). The P–T estimates show that wide ranges of provenance for the lherzolites (50–70 km), suggesting that the deep mantle column sampled by the lherzolites is homogenous. In Fig. 9, most

of the spinel lherzolites from this study display a trend subparallel to the slope of continental geotherm with heat flow between 60 and 90 mW/m^2 (Pollack and Chapman 1977), consistent with the average 70 mW/m^2 heat flows in the region (Morgan 1983; Čermák and Bodri 1991). Such high geothermal gradient than the normal continental gradient (40 mW/m^2, Pollack and Chapman 1977) reflects a thermal disturbance probably related to the presence of rising mantle plume in an active tectonic setting.

Timing of depletion and enrichment events of the lithospheric mantle

The Nd model ages for the spinel lherzolites of this study, calculated according to the depleted mantle model (T_{DM}) of Goldstein et al. (1984), provide some evidences on the timing of depletion in the mantle beneath Turkana Depression (Table 3). Samples HA6B, DM827, and TC01 show depleted MORB mantle (DMM) isotopic compositions, with very low $^{87}Sr/^{86}Sr$, high $^{147}Sm/^{144}Nd$, and high $^{143}Nd/^{144}Nd$ (Table 3; Fig. 7), which require long-time depletion of upper mantle. Assuming that these samples (HA6B, DM827, and TC01) are relatively unmodified or least affected by later processes, they represent the characteristics of the lithospheric mantle beneath Turkana Depression to estimate the minimum age of depletion; The T_{DM} model ages of the spinel lherzolites indicate an age of depletion between 1.07 and 0.83 Ga (Table 3, mean T_{DM} model age of 0.95 Ga) within the T_{DM} range of crustal rocks from southern Ethiopia (0.96–1.26 Ga; Teklay et al. 1998) and Kenya (0.69–1.98 Ga; Harris et al. 1984; Key et al. 1989). The similarity in depletion ages suggests that the lithosphere and the crust in these regions are differentiated from a common juvenile Neoproterozoic depleted mantle source (Woldemichael et al. 2009) during the Neoproterozoic crust-formation event (Stern 2002). According to Teklay et al. (1998), three periods of magmatism are recognized in southern Ethiopia on the basis of single zircon $^{207}Pb/^{206}Pb$ evaporation ages of the crust, at ~850, ~750–700, and ~650–550 Ma enclosed within the time span of Pan-African orogeny (950–450 Ma, Kröner 1984). Similarly, the Sm–Nd isochron of the three samples (HA6B, DM827, and TC01) also define a linear regression passing through the present-day depleted composition and gives an age of 996 Ma (Fig. 7b), consistent with the T_{DM} ages. The T_{DM} model ages obtained in this study are comparable to the T_{MA} and T_{RD} model ages (mean 1.1 Ga) on the same samples (Wang et al. 2005) but younger than from those ages obtained for Mega xenoliths (2.4–2.8 Ga; Reisberg et al. 2004). The latter age range shows a decoupling between the crust and the lithosphere, which might be related to the remnant of remobilized older (Archean) lithosphere or to the northward extension of Tanzanian cratonic lithosphere beneath in the region (Reisberg et al. 2004).

We consider that the lower and highly disturbed T_{DM} model ages have no age significant (Table 3). Sm–Nd isochron also show scattered correlation (Fig. 7b). Therefore, it is not possible to constrain the age of the metasomatic event. As discussed in Sect. 6.2, the lherzolites are metasomatised by the combined effect of hydrous fluid and silicate melt that have lower $^{143}Nd/^{144}Nd$ and higher $^{87}Sr/^{86}Sr$, consistent with the Kenya plume (Rogers et al. 2000) or plumelet containing a matrix of high-He type component with blobs of HIMU-like component (Meshesha and Shinjo 2008). However, as shown in Fig. 7, the metasomatised samples are characterized by slightly higher $^{143}Nd/^{144}Nd$ and lower $^{87}Sr/^{86}Sr$ than any plume-related volcanic rocks, suggesting that the metasomatic processes occurred shortly before the emplacement of any volcanic rocks in the region.

Conclusions

1. The studied mantle xenoliths are spinel lherzolites in composition with primary assemblages of olivine + orthopyroxene + clinopyroxene + spinel and characterized by a protogranular texture. They can be divided into two types: anhydrous and hydrous spinel lherzolites, the latter group characterized by the occurrences of pargasite and phlogopite.
2. The major element average composition of the studied peridotites (CaO = 3.80–5.55 wt%, Al_2O_3 = 2.46–4.12 wt%, and MgO = 34.68–38.13 wt%) is analogous to the composition of slightly depleted primitive mantle. In addition, the compositions of spinel (Cr# = 0.062–0.117, Al_2O_3 = 59.01–64.43 wt%) and clinopyroxene (Mg# = 88.4–91.7, Al_2O_3 = 5.18–6.67 wt%) indicate that the lherzolites are fertile and have not experienced significant partial melting and melt extractions.
3. The trace element compositions of clinopyroxene and whole-rock samples show flat (MREE-HREE) to slightly depleted (LREE) chondrite-normalized REE patterns. Only one sample (HA7A)that has amphibole vein contains LREE-enriched clinopyroxene and amphibole. Both types of spinel lherzolites are characterized by depleted $^{87}Sr/^{86}Sr$ (0.701796–0.702945) and high $^{143}Nd/^{144}Nd$ (0.512992–0.513478) with wide ranges of $^{206}Pb/^{204}Pb$ (17.86–19.68) isotopic compositions.
4. The occurrence of amphibole and phlogopite shows modal metasomatic effect in hydrous spinel lherzolites. Both types of spinel lherzolites have higher Ti/Eu and lower (La/Yb)n implying that the metasomatic

agent was silica-rich melt (or fluid) rather than carbonate-rich fluid. Therefore, the spinel lherzolites from Turkana Depression have experienced modal and cryptic metasomatism by the combined effect of hydrous fluid, and silicate melt infiltrated the lithosphere shortly before the emplacement of asthenospheric mantle plume.

5. The equilibrium temperature and pressure estimations yield 847–1,052°C and 15.6–22.2 kb corresponding to depths between 50 and 70 km. Most of the estimated P–T shows an elevated geotherm (60–90 mW/m^2) that is related to the presence of rising mantle plume in an active tectonic setting.
6. Sm–Nd isotopic systematic gives a mean T_{DM} model age of 0.95 Ga interpreted as the depletion age of the SCLM coincides with Neoproterozoic crustal evolution event in the region.

Acknowledgments D.M. strongly acknowledges support from Japan Society for Promotion of Science (JSPS) for postdoctoral fellowship program for foreign researcher. We appreciate S. Ohde (Univ. Ryukyus) for providing accesses to TIMS and ICP-MS. We are also grateful to the staffs of Geological Survey of Ethiopia (GSE) who had involved in collecting of the samples during the regional geological mapping of Yabello area. We thank the two reviewers, J. Blusztajn and T. Furman, for their constrictive comments that improved this paper. This work was supported by Grant-in-Aid for JSPS Fellows 21-09234 to R.S.

References

Arai S (1994) Characterization of spinel peridotites by olivine-spinel compositional relationships: review and interpretation. Chem Geol 113:191–204

Ayalew D, Yirgu G, Ketefo E, Barbey P, Ludden J (2003) Intrusive equivalents of flood volcanics: evidence from petrology of xenoliths in Quaternary Tana basanites. Ethiop J Sci 26:93–102

Ayalew D, Arndt N, Bastien F, Yirgu G, Kieffer B (2009) A new mantle xenolith locality from Simien shield volcano, NW Ethiopia. Geol Maga 146(1):144–149

Baker MB, Stolper EM (1994) Determining the composition of high-pressure mantle melts using diamond aggregates. Geochim Cosmochim Acta 58:2811–2827

Baker J, Chazot G, Menzies M, Thirlwall M (1998) Metasomatism of the shallow mantle beneath Yemen by the Afar plume-Implications for mantle plumes, flood volcanism, and intraplate volcanism. Geology 26:431–434

Bedini RM, Bodinier JL (1999) Distribution of incompatible trace elements between the constituents of spinel peridotite xenoliths: ICP-MS data from the East African Rift. Geochim Cosmochim Acta 63:3883–3900

Bedini RM, Bodinier JL, Dautria JM, Morten L (1997) Evolution of LILE-enriched small melt fractions in the lithospheric mantle: a case study from the East African Rift. Earth Planet Sci Lett 153:67–83

Benoit MH, Nyblade AA, Owens TJ, Stuart G (2006a) Mantle transition zone structure and upper mantle S velocity variations beneath Ethiopia: evidence for a broad, deep-seated thermal anomaly. Geochem Geophys Geosyst 7:Q11013. doi:10.1029/2006GC001398

Benoit MH, Nyblade AA, Pasyanos ME (2006b) Crustal thinning between the Ethiopian and East African plateaus from modeling Rayleigh wave dispersion. Geophys Res Lett 33:L13301. doi:10.1029/2006GL025687

Bjerg EA, Ntaflos T, Kurat G, Dobosi G, Labudía CH (2005) The upper mantle beneath Patagonia, Argentina, documented by xenoliths from alkali basalts. J S Am Earth Sci 18:125–145

Blusztajn J, Hart SR, Shimizu N, McGuire AV (1995) Trace-element and isotopic characteristics of spinel peridotite xenoliths from Saudi Arabia. Chem Geol 123:53–65

Bonini M, Corti G, Innocenti F, Manetti P, Mazzarini F, Abebe T, Pecskay Z (2005) Evolution of the Main Ethiopian Rift in the frame of Afar and Kenya rifts propagation. Tectonics 24:TC1007. doi:10.1029/2004TC001680

Boyd FR (1989) Compositional distinction between oceanic and cratonic lithosphere. Earth Planet Sci Lett 96:15–26

Boyd FR, Pokhilenko NP, Pearson DG, Mertzman SA, Sobolev NV, Finger LW (1997) Composition of the Siberian cratonic mantle: evidence from Udachnaya peridotite xenoliths. Contrib Mineral Petrol 128:228–246

Brey GP, Köhler TP (1990) Geothermobarometry in four phase lherzolites, II New thermometers, and practical assessment of existing thermometers. J Petrol 31:1353–1378

Čermák V, Bodri L (1991) A heat production model of the crust and upper mantle. Tectonophysics 194:307–323

Chen JC, Hsu CN, Ho KS (2003) Geochemistry of cenozoic volcanic rocks and related ultramafic xenoliths from the Jilin and Heilongjiang provinces, northeast China. J Asian Earth Sci 21:1069–1084

Coltorti M, Bonadiman C, Hinton RW, Siena F, Upton BGJ (1999) Carbonatite metasomatism of the oceanic upper mantle: evidence from clinopyroxenes and glasses in ultramafic xenoliths of Grande Comore, Indean Ocean. J Petrol 40:133–165

Conticelli S, Sintoni MF, Abebe T, Mazzarini F, Manetti P (1999) Petrology and geochemistry of ultramafic xenoliths and host basalts from the Ethiopian Volcanic Province: an insight into the upper mantle under Eastern Africa. In: Boccaletti M, Peccerillo A (eds) The Ethiopian rift system, vol 11. Acta Vulcanol pp 143–159

Davidson A (1983) The Omo River Project: reconnaissance geology and geochemistry of parts of Illubabor, Kefa, Gemu and Sidamo, Ethiopia, vol 2. Bull Ethiop Insti Geol Surv

Davidson A, Rex DC (1980) Age of volcanism and rifting in southwestern Ethiopia. Nature 283:657–658

Dawson JB (1984) Contrasting types of upper mantle metasomatism? In: Kornprobst J (ed) Kimberlites? Elsevier, Amsterdam, pp 289–294

Debayle E, Leveque JJ, Cara M (2001) Seismic evidence for a deeply rooted low-velocity anomaly in the upper mantle beneath the northeastern Afro/Arabian continent. Earth Planet Sci Lett 193:423–436

Deniel C, Vidal PH, Coulon C, Vellutini PJ, Piguet P (1994) Temporal evolution of mantle sources during continental rifting: the volcanism of Djibouti (Afar). J Geophys Res 99:2853–2869

DePaolo DJ, Wasserburg GJ (1976) Nd isotopic variations and petrogenetic models. Geophys Res Lett 3:249–252

Dugda MT, Nyblade AA, Julia J, Langston CA, Ammon CJ, Simiyu S (2005) Crustal structure in Ethiopia and Kenya from receiver function analysis. J Geophys Res 110:B01303. doi:10.1029/2006JB004918

Ebinger CJ, Sleep NH (1998) Cenozoic magmatism throughout East Africa resulting from impact of a single plume. Nature 395:788–791

Ebinger CJ, Bechtel TD, Forsyth DW, Bowin CO (1989) Effective elastic plate thickness beneath the East African and Afar Plateaus and dynamic compensation of the uplifts. J Geophys Res 94:2883–2901

Ebinger CJ, Yemane T, WoldeGebriel G, Aronson JL, Walter RC (1993) Late Eocene-Recent volcanism and faulting in southern main Ethiopian rift. J Geol Soc Lon 150:99–108

Ebinger CJ, Yemane T, Harding DJ, Tesfaye S, Kelley S, Rex DC (2000) Rift deflection, migration, and propagation: linkage of the Ethiopian and Eastern rifts, Africa. Geol Soc Am Bull 112:163–176

Ferrando S, Frezzotti ML, Neumann ER, Astis DG, Peccerillo A, Dereje A, Gezahegn Y, Teklewold A (2008) Composition and thermal structure of the lithosphere beneath the Ethiopian plateau: evidence from mantle xenoliths in basanites, Injibara, Lake Tana Province. Mineral Petrol 93:47–78

Franz L, Brey GP, Okrusch M (1996) Steady state geotherm, thermal disturbances, and tectonic development of the lower lithosphere underneath the Gibeon Kimberlite Province, Namibia. Contrib Mineral Petrol 126:181–198

Frey FA, Prinz M (1978) Ultramafic inclusions from San Carlos, Arizona: petrologic and geochemical data bearing on their petrogenesis. Earth Planet Sci Lett 38:129–176

Frezzotti ML, Ferrando S, Peccerillo A, Petrelli M, Tecce F, Perucchi A (2010) Chlorine-rich metasomatic H_2O-CO_2 fluids in amphibole-bearing peridotites from Injibara (Lake Tana region, Ethiopian plateau): nature and evolution of volatiles in the mantle of a region of continental flood basalts. Geochim Cosmochim Acta 74:3023–3039

Furman T, Bryce J, Karson J, Iotti A (2004) East African Rift system (EARS) plume structure: insights from Quaternary mafic lavas of Turkana, Kenya. J Petrol 45:1069–1088

Furman T, Bryce J, Rooney T, Hanan B, Yirgu G, Ayalew D (2006a) Heads and tails. In: Yirgu G, Ebinger CJ, Maguire PKH (eds) 30 million years of the Afar plume, vol 259. Geol Soc Spec Publ London, pp 95–119

Furman T, Kaleta K, Bryce J, Hanan B (2006b) Tertiary Mafic Lavas of Turkana, Kenya: constraints on East African Plume structure and the occurrence of high-μ volcanism in Africa. J Petrol 47:1221–1244

George R, Rogers N (2002) Plume dynamics beneath the African plate inferred from the geochemistry of the Tertiary basalts of southern Ethiopia. Contrib Mineral Petrol 144:286–304

George R, Rogers N, Kelley S (1998) Earliest magmatism in Ethiopia: evidence for two mantle plumes in one flood basalt province. Geology 26:923–926

Glücklich ME, Mercier JC (1989) The Basin-and-Range lithospheric mantle: evidence for homogeneity at the regional scale. TERRA Abstr 1:318

Goldstein SL, O'Nions RK, Hamilton PJ (1984) A Sm-Nd isotopic study of atmospheric dusts and particulates from major river systems. Earth Planet Sci Lett 70:221–236

Grégoire M, Bell DR, le Roex AP (2003) Spinel lherzolite xenoliths from the Kaapvaal craton (South Africa): trace element evidence for a metasomatic history. J Petrol 44:629–657

Grégoire M, Tinguely C, Bell DR, le Roex AP (2005) Spinel lherzolite xenoliths from the Premier kimberlite (Kaapvaal craton, South Africa): nature and evolution of the shallow upper mantle beneath the Bushveld complex. Lithos 84:185–205

Harris NBW, Hawkesworth CJ, Ries AC (1984) Crustal evolution in north-east and east Africa from model Nd ages. Nature 309:773–776

Hart SR (1984) A large scale isotope anomaly in the southern hemisphere mantle. Nature 309:753–757

Hart SR, Zindler A (1986) In search of bulk Earth composition. Chem Geol 57:247–267

Hirose K, Kushiro I (1993) Partial melting of dry peridotites at high pressures: determination of compositions of melts segregated from peridotite using aggregates of diamond. Earth Planet Sci Lett 114:477–489

Imai N, Terashima S, Itoh S, Ando A (1995) 1994 compilation of analytical data for minor and trace elements in seventeen GSJ geochemical reference samples, "igneous rock series". Geostand Newsl 19:135–213

Ionov DA, Hofmann AW (1995) Nb-Ta-rich mantle amphiboles and micas: implications for subduction-related metasomatic trace element fractionations. Earth Planet Sci Lett 131:341–356

Jacobsen SB, Wasserburg GJ (1980) Sm-Nd isotopic evolution of chondrites. Earth Planet Sci Lett 50:139–155

Jagoutz E, Palme H, Blum H, Cendales M, Dreibus G, Spettel B, Lorenz V, Wänke H (1979) The abundances of major, minor and trace elements in the Earth's mantle as derived from primitive ultramafic nodules. In: Proceeding of 10th lunar planetary science conference, vol 10. Geochim Cosmochim Acta Supplement, pp 2031–2051

Janney PE, Le Roex AP, Carlson RW, Viljoen KS (2002) A chemical and multi-isotope study of the Western Cape melilitite province, South Africa: implications for the sources of kimberlites and the origin of the HIMU signature in Africa. J Petrol 43:2339–2370

Kaeser B, Kalt A, Pettke T (2006) Evolution of the lithospheric mantle beneath the Marsabit volcanic field (northern Kenya): constraints from textural, P-T and geochemical studies on xenoliths. J Petrol 47:2149–2184

Key RM, Charsley TJ, Hackman BD, Wilkinson AF, Rundle CC (1989) Superimposed upper proterozoic collision-controlled orogenies in the Mozambique orogenic belt of Kenya. Precambr Res 44:197–225

Köhler TP, Brey GP (1990) Calcium exchange between olivine and clinopyroxene calibrated as a geothermobarometer for natural peridotites from 2 to 60 kb with applications. Geochim Cosmochim Acta 54:2375–2388

Kröner A (1984) Late Precambrian plate tectonics and orogeny: a need to redefine the term Pan-African. In: Klerkx J, Michot J (eds) African geology. Musee Royal L'Afrique Centrale, Tervuren, pp 23–28

Leake BE, Woolley AR, Arps CES, Birch WD, Gilbert MC, Grice JD, Hawthorne FC, Kato A, Kisch HJ, Krivovichev VG, Linthout K, Laird J, Mandarino JA, Maresch WV, Nickel EH, Rock NMS, Schumacher JC, Smith DC, Stephenson NCN, Ungaretti L, Whittaker EJW, Youzhi G (1997) Nomenclature of amphiboles: report of the subcommittee on amphiboles of the international mineralogical association, commission on new minerals and mineral names. Can Mineral 35:219–246

Lorand JP, Reisberg L, Bedini RM (2003) Platinum-group elements and melt percolation processes in Sidamo spinel peridotite xenoliths, Ethiopia, East African Rift. Chem Geol 196:57–75

Maaløe S, Aoki KI (1977) The major element composition of the upper mantle estimated from the com position of lherzolites. Contrib Mineral Petrol 63:161–173

MacKenzie JM, Canil D (1998) Composition and thermal evolution of cratonic mantle beneath the central Achaean Slave Province, NWT, Canada. Contrib Mineral Petrol 134:313–324

McDonough WF (1990) Constraints on the composition of the continental lithospheric mantle. Earth Planet Sci Lett 101:1–18

McDonough WF, Sun SS (1995) The composition of the Earth. Chem Geol 120:223–253

Mechie J, Keller GR, Prodehl C, Khan MA, Gaciri SJ (1997) A model for the structure, composition and evolution of the Kenya rift. Tectonophysics 278:95–119

Mercier JC (1980) Single-pyroxene thermobarometry. Tectonophysics 70:1–37

Mercier JC, Nicolas A (1975) Textures and fabrics of upper mantle peridotites as illustrated by xenoliths from basalts. J Petrol 16:454–487

Meshesha D, Shinjo R (2008) Rethinking geochemical feature of the Afar and Kenya mantle plumes and geodynamic implications. J Geophys Res 113:B09209. doi:10.1029/2007JB005549

Michard A, Gurriet P, Soudant M, Albarede F (1985) Nd isotopes and French Phanerozoic shales: external vs. internal aspects of crustal evolution. Geochim Cosmochim Acta 49:601–610

Morgan P (1983) Constraints on rift thermal processes from heat flow and uplift. Tectonophysics 94:277–298

Morten L, Defrancesco AM, Bonavia FF, Haileselassie G, Bargossi GM, Bondi M (1992) A new mantle xenolith locality from Southern Ethiopia. Mineral Maga 56:422–425

Niu Y (2004) Bulk-rock major and trace element compositions of abyssal peridotites: implications for mantle melting, melt extraction and post-melting processes beneath Mid-Ocean Ridges. J Petrol 45:2423–2458

Niu Y, Hékinian R (1997) Basaltic liquids and harzburgitic residues in the Garrett transform: a case study at fast-spreading ridges. Earth Planet Sci Lett 146:243–258

Norman MD (1998) Melting and metasomatism in the continental lithosphere: laser ablation ICPMS analysis of minerals in spinel lherzolites from eastern Australia. Contrib Mineral Petrol 130:240–255

Nyblade AA, Owens TJ, Gurrola H, Ritsema J, Langston CA (2000) Seismic evidence for a deep upper mantle thermal anomaly beneath east Africa. Geology 28:599–602

Pollack HN, Chapman DS (1977) Regional variation of heat flow, geotherms, and lithospheric thickness. Tectonophysics 38:279–296

Raczek I, Stoll B, Hofmann AW, Jochum KP (2001) High-precision trace element data for the USGS reference materials BCR-1, BCR-2, BHVO-1, BHVO-2, AGV-1, AGV-2, DTS-1, DTS-2, GSP-1 and GSP-2 by ID-TIMS and MIC-SSMS. Geostand Newsl 25:77–86

Reisberg L, Lorand JP, Bedini RM (2004) Reliability of Os model ages in pervasively metasomatized continental mantle lithosphere: a case study of Sidamo spinel peridotite xenoliths (East African Rift, Ethiopia). Chem Geol 208:119–140

Rivalenti G, Vannucci R, Rampone E, Mazzucchelli M, Piccardo GB, Piccirillo EM, Bottazzi P, Ottolini L (1996) Peridotite clinopyroxene chemistry reflects mantle processes rather than continental versus oceanic settings. Earth Planet Sci Lett 139:423–437

Roger S, Pik R, Dautria JM, Coulon C, Yirgu G, Ayalew D, Legros P (1997) Rifting actif ou passif en Ethiopie? Elements de reponse apportes par l'etude des xenolites peridotitiques de la region du lac Tana [Active or passive rifting in Ethiopia? Contribution of peridotitic xenoliths from the Lake Tana area]. Comptes Rendu de l'Academie des Sciences de Paris 324:1009–1016

Roger S, Dautria JM, Coulon C, Pik R, Yirgu G, Michard A, Legros P, Ayalew D (1999) An insight on the nature, composition and evolution of the lithospheric mantle beneath in the north-western Ethiopian plateau: the ultrabasic xenoliths from the Tana Lake Province. In: Boccaletti M, Peccerillo A (eds) The Ethiopian rift system, vol 11. Acta Vulcanol, pp 161–168

Rogers N, MacDonald R, Fitton JG, George R, Smith M, Barreiro B (2000) Two mantle plumes beneath the East African rift system: Sr, Nd and Pb isotope evidence from Kenya rift basalts. Earth Planet Sci Lett 176:387–400

Rooney TO, Furman T, Yirgu G, Ayalew D (2005) Structure of the Ethiopian lithosphere; xenolith evidence in the main Ethiopian Rift. Geochim Cosmochim Acta 69:3889–3910

Rudnick RL, McDonough WF, Chappell BC (1993) Carbonatite metasomatism in the northern Tanzanian mantle. Earth Planet Sci Lett 114:463–475

Schilling M, Conceiçõ RV, Mallmann D, Koester E, Kawashita K, Hervé F, Morata D, Motoki A (2005) Spinel-facies mantle xenoliths from Cerro Redondo, Argentine Patagonia: Petrographic, geochemical, and isotopic evidence of interaction between xenoliths and host basalt. Lithos 82:485–502

Shaw JE, Baker J, Kent AJR, Ibrahim KM, Menzies MA (2007) The geochemistry of the Arabian lithosphere mantle-a source for intraplate volcanism? J Petrol 48:1495–1512

Shinjo R, Matsumura R (2006) Geochemical characteristics of mantle xenoliths from quaternary alkaline lavas, southern Ethiopia. Geochim Cosmochim Acta 70 (18):A37. doi:10.1016/j.gca.2006.06.1090 (Supplementary 1)

Shinjo R, Woodhead JD, Hergt JM (2000) Geochemical variation within the northern Ryukyu Arc: magma source compositions and geodynamic implications. Contrib Mineral Petrol 140:263–282

Shinjo R, Chekol T, Meshesha D, Tatsumi Y, Itaya T (2010) Geochemistry and geochronology of the mafic lavas from the southeastern Ethiopian rift (the East African Rift System): assessment of models on magma sources, plume-lithosphere interaction and plume evolution. Contrib Mineral Petrol. doi:10.1007/s00410-010-0591-2

Stern RJ (2002) Crustal evolution in the East African Orogen: a neodymium isotopic perspective. J Afr Earth Sci 34:109–117

Stern RJ, Johnson P (2010) Continental lithosphere of the Arabian Plate: a geologic, petrologic, and geophysical synthesis. Earth-Sci Rev 101:29–67

Stewart K, Rogers N (1996) Mantle plume and lithosphere contributions to basalts from southern Ethiopia. Earth Planet Sci Lett 139:195–211

Sun SS, McDonough WF (1989) Chemical and isotopic systematics of oceanic basalts: implications for mantle composition and processes. In: Saunders AD, Norry MJ (eds) Magmatism in the ocean basins, vol 42. Geol Soc Spec Publ, pp 313–345

Teklay M, Kröner A, Mezger K, Oberhänsli R (1998) Geochemistry, Pb-Pb single zircon ages and Nd-Sr isotope composition of Precambrian rocks from southern and eastern Ethiopia: implications for crustal evolution in East Africa. J African Earth Sci 26:207–227

Teklay M, Scherer EE, Mezger K, Danyushevsky L (2010) Geochemical characteristics and Sr-Nd-Hf isotope compositions of mantle xenoliths and host basalts from Assab, Eritrea: implications for the composition and thermal structure of the lithosphere beneath the Afar Depression. Contrib Mineral Petrol 159:731–751

Wang KL, Chung SL, O'Reilly SY, Sun SS, Shinjo R, Chen CH (2004) Geochemical constraints for the genesis of post-collisional magmatism and the geodynamic evolution of the northern Taiwan region. J Petrol 45:975–1011

Wang KL, O'Reilly SY, Griffin WL, Pearson NJ, Matsumura R, Shinjo R (2005) Proterozoic mantle lithosphere beneath the East African Rift (Southern Ethiopia): In situ Re-Os evidence. Geochim Cosmochim Acta 69 (10):A284 (Supplementary 1)

Wells PRA (1977) Pyroxene thermometry in simple and complex systems. Contrib Mineral Petrol 62:129–139

Wilshire HG, Shervais JW (1975) Al-augite and Cr-diopside ultramafic xenoliths in basaltic rocks from western United States. Phys Chem Earth 9:257–272

Witt-Eickschen G, Seck HA (1991) Solubility of Ca and Al in orthopyroxene from spinel peridotite: an improved version of an empirical geothermometer. Contrib Mineral Petrol 106:431–439

WoldeGabriel G, Aronson JL, Walter RC (1990) Geology, geochronology and rift basin development in the central sector of the Main Ethiopia Rift. Geol Soc Am Bull 102:439–458

WoldeGabriel G, Yemane T, Suwa G, White T, Asfaw B (1991) Age of volcanism and rifting in the Burjji-Soyoma area, southern Main Ethiopian rift, Geo- and biochronolgic data. J Afr Earth Sci 13:437–447

Woldemichael BW, Kimura J-I, Dunkley DJ, Tani K, Ohira H (2009) SHRIMP U-Pb zircon geochronology and Sr-Nd isotopic systematic of the Neoproterozoic Ghimbi-Nedjo mafic to intermediate intrusions of Western Ethiopia: a record of passive margin magmatism at 855 Ma? Int J Earth Sci (Geol Rundsch) 99:1773–1790

Wyllie PJ (1981) Plate tectonics and magma genesis. Geol Rundsch 70:128–153

Xu X, O'Reilly SY, Griffin WL, Zhou X (2003) Enrichment of upper mantle peridotite: petrological, trace element and isotopic evidence in xenoliths from SE China. Chem Geol 198:163–188

Yemane T, WoldeGebriel G, Tesfaye S, Berhe SM, Durary S, Ebinger CJ, Kelley S (1999) Temporal and geochemical characteristics of Tertiary Volcanic Rocks and tectonic history in the southern main Ethiopia Rift and the adjacent volcanic fields. Acta Vulcanol 11:99–119

Zanettine B, Justin-Visentin E, Nicoletti M, Petrucciani C (1978) The evolution of the Chencha escarpment and the Ganjuli graben (lake Abaya) in the southern Ethiopian rift. Neues Jahrbuch fur Geologie und Palaentologie, Monatsh 8:473–490

Zindler A, Hart SR (1986) Chemical Geodynamics. Annu Rev Earth Planet Sci Lett 14:493–571